Cardioprotective effects of α-cardiac actin on oxidative stress in a dilated cardiomyopathy mouse model

Aude Angelini, Mark-alexander Gorey, Florent Dumont, Nathalie Mougenot, Maria Chatzifrangkeskou, Antoine Muchir, Zhenlin Li, Mathias Mericskay, Jean-francois Decaux

Cardioprotective effects of α-cardiac actin on oxidative stress in a dilated cardiomyopathy mouse model

Angelini, A[1]., Gorey, M. A[1]., Dumont, F[2]., Mougenot, N[3]., Chatzifrangkeskou, M[4]., Muchir, A[4]., Li, Z[1]., Mericskay, M[2] & Decaux, J.F[1].

[1] Sorbonne Université, Institut de Biologie Paris-Seine (IBPS), CNRS UMR 8256, INSERM ERL U1164, Biological Adaptation and Ageing, 75005, Paris, France

[2] Université Paris-Saclay, INSERM UMR-S 1180, Signalling and Cardiovascular Pathophysiology, 92296, Châtenay-Malabry, France

[3] Sorbonne Université, INSERM UMS 28 Phénotypage du petit animal, Faculté de Médecine, Pierre et Marie Curie, 75013, Paris, France.

[4] Sorbonne Université, INSERM UMRS 974, Center of Research in Myology, Institut de Myologie, Paris, France

Corresponding author : zhenlin.li@sorbonne-universite.fr

Phone: +33 1 44 27 21 36

Running title: cardioprotective effect of α-cardiac actin

None standard abbreviations used in the manuscript

ANF: **A**trial **N**atriuretic **F**actor

ARP-WASP: **A**ctin-**R**elated **P**rotein-**W**iskott-**A**ldrich Syndrome Protein

CAG: Synthetic promoter constructed from the **C**ytomegalovirus (CMV) early enhancer element, chicken beta-**A**ctin promoter and the splice acceptor of the rabbit beta-**G**lobin gene

CardAct: α-**Card**iac **Act**in

CAT: **C**hloramphenicol **A**cetyl **T**ransferase

Cre: **Cre** recombinase

Cy5: **Cy**anine-derived fluorophore 5

DAPI: 4′, 6-**D**i**A**midino-2-**P**henyl**I**ndole

DCM: **D**ialted **C**ardio**M**yopathy

DEG: **D**atabase of **E**ssential **G**enes

DHE: **D**i**H**ydro**E**thidium

DIGE: **D**ifferential **I**n-**G**el **E**lectrophoresis

DMEM: **D**ubecco's **M**odified **E**ssential **M**edium

DNP: **D**i**N**itro**P**henol

DNPH: **D**i**N**itro**P**henyl**H**ydrazin

DTT: **D**i**T**hio**T**hreitol

EDTA: **E**thylene**D**iamine**T**etraacetic **A**cid

EF: **E**jection **F**raction

ER: **E**strogen **R**eceptor

ETC: **E**lectron **T**ransport **C**hain

F-Actin: **F**ilamentous **Actin**

FBS: **F**etal **B**ovine **S**erum

FITC: **F**luorescein **I**so**T**hio**C**yanate

Flx: **fl**oxed

G-Actin: **G**lobular **Actin**

GSEA: **G**ene **S**et **E**nrichment **A**nalysis

HEK293: **H**uman **E**mbryonic **K**idney 293 cells

HW/BW: **H**eart **W**eight/**B**ody **W**eight

LoxP: **Lo**cus of **X**-over **P**1which is a binding site of Cre recombinase

LV: **L**eft **V**entricle

MADS: **M**CM1- **A**GAMOUS- **D**EFICIENS- **S**RF

MCK: **M**uscle **C**reatine **K**inase

Mer: **M**utated **e**strogen **r**eceptor

MHC: **M**yosin **H**eavy **C**hain

MHz: **M**ega**H**ert**Z**

Myl: **My**osin **l**ight chain

NADPH: **N**icotinamide **A**denine **D**inucleotide **P**hosphate **H**ydrogen

NOX: **N**icotinamide adenine dinucleotide phosphate **OX**idase

NT: u**NT**reated cells

PAGE: **P**oly**A**crylamide **G**el **E**lectrophoresis

PBS: **P**hosphate **B**uffer **S**olution

PCR: **P**olymerase **C**hain **R**eaction

PI3K/AKT: **P**hosphatidyl**I**nositol-**3**-**K**inase **A**nd protein **K**inase B

PolyA: **PolyA**denylation signal

PS: **P**enicillin-**S**treptomycin

RT-qPCR: **R**eal-**T**ime **q**uantitative **P**olymerase **C**hain **R**eaction

LVFWd: **L**eft **V**entricle **F**ree **W**all diastolic

LVFWs: **L**eft **V**entricle **F**ree **W**all **s**ystolic

ROS: **R**eactive **O**xygen **S**pecies

RV: **R**ight **V**entricle

Sa: **S**ystolic velocity at mitral **A**nnulus

SDS: **S**odium **D**odecyl **S**ulfate

Sf: **S**RF-**f**loxed locus

SOD2: **S**uper**O**xide **D**ismutase **2**

Spw: **S**ystolic velocity **P**osterior **W**all

SRF: **S**erum **R**esponse **F**actor

SRF^{HKO}/CA: SRF **H**eart-specific **K**nock-**O**ut and -**C**ardiac **A**ctin transgen overexpression

STARS: **ST**riated muscle **A**ctivator of **R**ho **S**ignalling/actin-binding Rho activating protein

SYBR: An asymmetrical cyanine dye binding to DNA

TGCRE: **T**rans**G**enic mouse expressing -MHC-Mer**Cre**Mer

TGCA: **T**rans**G**enic mouse expressing -**C**ardiac **A**ctin

Tg-r-ACTC1: **T**rans**g**enic mouse expressing **r**at -cardiac actin (**ACTC1**)

UTC: **U**rea-**T**hiourea-**C**hap buffer

Vcfc: Shortening of **V**elocity of **C**ircumferential **F**ibers **C**orrected for heart rate

VDAC: **V**oltage-**D**ependent **A**nion **C**hannel

Summary

The expression of α-cardiac actin, a major constituent of the cytoskeleton of cardiomyocytes, is dramatically decreased in a mouse model of dilated cardiomyopathy triggered by inducible cardiac-specific serum response factor (*Srf*) gene disruption that could mimic some forms of human dilated cardiomyopathy. To investigate the consequences of the maintenance of α-cardiac actin expression in this model, we developed a new transgenic mouse based on Cre/LoxP strategy, allowing together the induction of SRF loss and a compensatory expression of α-cardiac actin. Here we report that maintenance of α-cardiac actin within cardiomyocytes temporally preserved cytoarchitecture from adverse cardiac remodelling through a positive impact on both structural and transcriptional levels. These protective effects were accompanied *in vivo* by the decrease of ROS generation and protein carbonylation and the down-regulation of NADPH oxidases NOX2 and NOX4. We also show that ectopic expression of α-cardiac actin protects HEK293 cells against oxidative stress induced by H_2O_2. Oxidative stress plays an important role in the development of cardiac remodelling and contributes also to the pathogenesis of heart failure. Taken together, these findings indicate that α-cardiac actin could be involved in the regulation of oxidative stress that is a leading cause of adverse remodelling during dilated cardiomyopathy development.

Key words

α-cardiac actin, dilated cardiomyopathy, oxidative stress, cardiac remodelling

Introduction

Sarcomere integrity is a common and crucial denominator in both skeletal and cardiac striated muscles. This often fails in a large number of inherited myopathies or cardiomyopathies. Among these various pathological disorders, dilated cardiomyopathy (DCM) represents the most common type of non-ischemic cardiomyopathies which is characterized by dilation and contractile dysfunction of the left and right ventricles associated with functional alterations leading to heart failure (1, 2). During DCM development, cardiomyocytes with an altered shape, a reduction in contractile force of the sarcomeres and a conduction disruption are usual features at the cellular scale, rushing towards deleterious cardiac remodelling (3, 4). The slow advances in the pharmacological treatment of patients suffering from DCM, lead to a high level of mortality and this disease still represents the main need for cardiac transplantation (5, 6).

Several clinical cases of familial DCM are linked with mutations in sarcomeric protein genes including the α-cardiac actin (Actc1) (7-9). In the adult mammalian myocardium, α-cardiac actin is the most represented among the four tissue-restricted muscular actin isoforms (10-12). Previous studies using *Actc1* -/- mouse model demonstrated that lack of α-cardiac actin is lethal during the perinatal period, in cause of myofibrillar disorganization leading to severe heart defects (13). In addition, overexpression of non-muscular γ-actin isoform only partially rescues *Actc1* -/- phenotype, which thus validates the specificity of α-cardiac actin isoform to ensure cardiac function (13). However, although α-cardiac actin holds a key role during myogenesis and especially in cardiomyogenesis, its involvement in mature myocardial physiology and/or pathophysiology still remains hardly assessable.

In our laboratory, a mouse model of DCM was developed by the Cre/loxP method. Named SRF ^{HKO}, this model leads to cardiac-specific and tamoxifen-inducible disruption of the Serum Response Factor (*Srf*) gene (4, 14). SRF is a MADS-Box transcription factor binding to CArG-box, especially abundant in the cardiac muscle. Many of its 160 putative target genes are involved in cardiac muscle development and function (15). Among them, *Actc1* which holds four CArG-boxes within its promoter, is a major SRF target gene (16). Indeed, our previous studies demonstrated that *Actc1* was among the first gene whose expression was drastically decreased in response to SRF disruption (4, 14) followed by a progressive reduction in the amount of α-cardiac actin protein down to 50% at day 45 after the loss of SRF and the death of the animals around day 60 (17). Under such drastic conditions, it was

difficult to distinguish the events due to SRF loss from those due to α-cardiac actin loss. Here, we used a new transgenic mouse model also based on Cre/LoxP strategy, allowing together the induction of SRF loss and a compensatory expression of α-cardiac actin (called SRF ^{HKO}/CA). We show that a supply of α-cardiac actin in SRF ^{HKO} mice measurably preserves a broad range of functional, mechanical and transcriptional aspects, delaying DCM development. We also provide evidence that α-cardiac actin holds some protective effects against oxidative stress by *in vivo* and *in vitro* approaches. Altogether, our results reveal the crucial role of α-cardiac actin in the development of DCM and highlighted for the first time its involvement in cardiac muscle redox regulation.

Materials and Methods

Transgenic mice

All animal care and experimental procedures were conducted according to the Ministere de l'Enseignement Superieur et de la Recherche and approved by the veterinary department of Paris to the legislation of R214-87 to R214-122 and R215-10 articles with the authorization number 75–835. All experimental procedures were done in accordance with institutional guidelines for animal experimentation.

Inducible α-cardiac actin overexpression mice were generated using a transgene CAG-*flx*-CAT-*flx*-Actc1 in which a rat *Actc1* cDNA is placed downstream to a floxed cassette containing a chloramphenicol acetyl transferase (CAT) reporter gene and a polyadenylation (PolyA) signal sequence that terminates transcription. The expression is under the control of the ubiquitous composite promoter made of cytomegalovirus immediate early enhancer and the chicken β-actin promoter. The *Actc1* transgenic strain was backcrossed at least five times onto a C57BL/6N genetic background and then were crossed with α-*MHC-MerCreMer* mice abbreviated TGCRE to generate *the Actc1* transgenic mice (α-*MHC-MerCreMer: CAG-Actc1*) abbreviated TGCA. It is only in the presence of Cre which excises the CAT-PolyA sequence that α-cardiac actin can be expressed. Three transgenic lines were obtained and the line with the highest induction of the transgene (2.4 folds) was kept for the next crossings (Fig. S1E).

The selected *Actc1* transgenic strain was crossed with mice homozygous for floxed *Srf* alleles (*Sf/Sf*) to generate *CAG-Actc1*: *Sf/Sf* mice (*loxP-CAT-loxP-CardAct*: *Sf/Sf*) (Fig. 1). The *CAG-Actc1*: *Sf/Sf* mice were crossed with α-*MHC-MerCreMer: Sf/Sf* mice (abbreviated *SRF* ^{HKO}) to generate the experimental groups: controls (*Sf/Sf*), cardiac inducible *SRF* ^{HKO} (α-*MHC-MerCreMer*: *Sf/Sf*) and cardiac SRF ^{HKO}/*CA* inducible mutant (α-*MHC-MerCreMer: loxP-CAT-loxP-CardAct: Sf/Sf*) (Fig. 1). These three groups of mice were systematically included

in all experiments. Mice were selected on the basis of PCR genotyping analysis of tail DNA. For all experiments, 2-month-old mice (including male and female mice per group) were injected by intraperitoneal with 1 mg of tamoxifen (Sigma) in 50 µL of sunflower oil for 4 consecutive days. Analyses were performed at day 0, 30, 35 or 45 according to the experiments.

Echocardiography

Echocardiography was performed as previously described (18) using echocardiography-Doppler (GE Medical System Co, Vivid 7 Dimension/Vivid7 PRO) with an ultrasound probe frequency range from 9 to 14 MHz. The mice were lightly anesthetized under isoflurane (induction with 2% isoflurane-100% O_2, and maintained with 0.2% isoflurance-100% O_2) with spontaneous ventilation. A blinded experimenter, unaware of the genotype performed the examinations.

Histological, immunochemistry and morphometrical analyses

Cardiac morphology was evaluated by hematoxylin-eosin staining on frozen cardiac cross sections. Immunofluorescence analysis of frozen sections involved the primary antibody anti-SRF (1:500, Santa Cruz) followed by Alexa-Fluor-594-coupled secondary antibody and FITC-coupled-anti-vinculin (1:500, Sigma). Alexa-Fluor-594 phalloidin (1:1000, Sigma) was used to detect polymerized actin. HEK293 cells were seeded onto gelatin coated slides for the *in vitro* immunochemistry analysis. To detect α-cardiac actin overexpression, an anti-α-cardiac actin antibody (1:150, American Research Products) was used followed by a Cy3-coupled secondary antibody. Alexa-Fluor-488 phalloidin (1:1000, Sigma) was used to visualize polymerized actin. Nuclei were counterstained with DAPI dye (1:10000, ThermoScientific).

The maximal length and width of cardiomyocytes were measured by confocal microscopy following vinculin-immunofluorescence staining using ImageJ software (version 1.49). Fifteen to 20 fields corresponding to more than 200 cardiac cells per group of mice were analyzed. Measurements were performed on samples from at least three individuals in each group.

DHE staining and detection of carbonylated protein on cardiac cross section

Superoxide production and DNA breaks were detected by dihydroethidium (DHE) staining (Sigma Aldrich). Frozen heart cross sections (8 µm thick) and fixed HEK293 cells were

incubated with 10 µM DHE for 75 min at 37°C in a dark humidified chamber. DHE signal was detected with a confocal laser scanning microscope Leica SP5 at 508 and 608 nm corresponding to the excitation and the emission wavelengths respectively.
Detection of carbonylated groups was performed on frozen cardiac cross section using oxiblot detection kit (Merck Millipore). After derivatization reaction, antibody anti-DNP then Cy3-coupled secondary antibody were used to detect dinitrophenylhydrazin (DNPH) signal.

Electron microscopy

Electron microscopy was performed on hearts of control, SRF ^{HKO}, SRF ^{HKO}/ CA mice as previously described (19). This study was done at the Cochin Institute Microscopy Core facility (Paris, France).

Isolation of heart mitochondria

Isolation of mitochondria was performed as previously described (20). Briefly, mitochondria were isolated from hearts of each group of mice by homogenization in an ice-cold glass Dounce homogenizer in a buffer A (100 mM sucrose, 50 mM Tris, 10 mM EDTA [pH 7.4]) containing protease inhibitors. After several washings and centrifugations, the pellet was rinced twice in a buffer B (300 mM sucrose, 5 mM Tris, 2 mM EDTA [pH 7.4]) containing protease inhibitors and further purified on self-forming Percoll gradients (33% [wt/vol] Percoll in sucrose buffer B). Purified mitochondria were rinsed twice in sucrose buffer B, and the protein concentration was determined by the Bradford's method using BSA as a standard (21).

Western blot analysis

Western blotting was performed as previously described (22) using anti-SRF (1:800, SantaCruz), anti-α-cardiac actin (1:1000, American Research Products), anti-ANF (1:800, Biorbyt), anti-MCK (1:500, SantaCruz), anti-Serca2 (1:1000, SantaCruz), anti-Complex IV subunit IV (1:500, Invitrogen), anti-Sirtuin3 (1:800, Cell Signaling), anti-SOD2 (1:200, Abcam), anti-VDAC1 (1:1000, Abcam), anti-aconitase2 (1:2000, Abcam), anti-NOX2 and anti-NOX4 (1:1000, Abcam) antibodies diluted in 5% bovine serum albumin. Antibodies against GAPDH (1:2000, Sigma) and anti-NDUFA9 (1:1000, Abcam) were used as loading control for total and for mitochondrial proteins respectively. IRDye secondary antibodies (1:5000, Li-Cor) were incubated in 5% milk. Infrared fluorescent signal was detected in Odyssey imaging system and quantified using ImageJ software.

To detect αMHC and βMHC isoforms in hearts, the migration of proteins was performed as previously described (23) following by a silver staining (24). The presence of glycerol in the gel allowed to separate MHC isoforms with different apparent molecular masses.

Quantification of F-actin and G-actin

The ratio of globular (G-) to filamentous (F-) actin was determined using a F-actin/G-actin assay kit (catalog number: BK 037, Cytoskeleton, Inc) according to manufacture's instructions. Briefly, 2 mg of cardiac tissue were homogenized in a lysis and F-actin stabilization buffer (LAS2) and then centrifuged at 2000 rpm for 5 min. F-actin was separated from G-actin by centrifugation at 100.000 g for 60 min at 37 °C. The F-actin-containing pellet was resuspended in F-actin depolymerizing buffer at a volume equivalent to the G-actin-containing supernatant volume. The resuspended F-actin pellet was kept on ice for 60 min with mixing by pipette every 15 min to dissociate F-actin. Proteins in equivalent volumes (10 µL) of supernatant and pellet were separated by SDS-PAGE and subjected to immunoblot analysis using an anti-pan actin antibody supplied in the kit. F/G actin ration was quantified using ImageJ solfware.

Detection of total carbonylated proteins

Myocardial tissues were dissolved in UTC Buffer composed with 8 M Urea, 2 M ThioUrea, 1% Chaps, 10 mM DTT. Proteins (10 µg) were incubated with Cy5-coupled monohydrazid (Sigma) to label free carbonyl groups of oxidized proteins. After loading and protein migration in 10% SDS-PAGE gel, Cy5 fluorescent signal was detected by Ettan DIGE imaging system and quantified using ImageJ software. The SDS-PAGE gel was normalized by total protein staining with Coomassie blue.

Quantitative RT-PCR

Total RNAs were extracted from nitrogenized hearts using RNA Now kit (bioPLUS) in accordance with the manufacturer's protocol. Reverse transcription was performed with High Capacity cDNA kit (Applied Biosystem). PCR analysis was done with SYBR Green PCR technology (Roche). NCBI primer blast online program was used to select and to design primers (available on request). *Gapdh*, *Cyclophilin A* and *Sdha* genes were selected as reference transcripts, regarding to preliminary GeNorm software analyses. Normalization was done using the geometrical average of *Cp* ratio from reference transcripts.

Gene microarray analyses

Total RNAs were hybridized on microarray Affymetrix U133A chips with 22.976 probe pairs. Statistical analyses were performed by the Cochin Institute Genomic Core facility (Paris, France). Data were normalized with Bioconductor software and tested by non-supervised approach with Principal Component Analysis. ANOVA statistical analysis was performed to extract DEGs with Partek DEG©. To highlight the most relevant pathways and genes, bioinformatic analyses were achieved with Ingenuity Pathway Analysis. Considering that we proceeded to cross-comparisons of the datasets and adopt a gene set enrichment analysis (GSEA) that include the calculation of normalized enrichment scores for each set and a false discovery rate, we selected the initial list of probe sets for each data simply on the criteri at P-value < 0.05. We deleted from the GSEA analyses, the probe set corresponding to the estrogen receptor alpha (ERalpha) that recognizes the Mer domain of the MerCreMer cDNA since transgene expression level largely overrides the endogenous ERalpha expression level and MerCreMer does not mediate the biologicial action of ERalpha.

Cell culture, transfection assays and stress induction by H_2O_2

HEK293 cells were cultured in Dubecco's modified essential medium (DMEM) containing 10% fetal bovine serum (FBS), 2 mM glutamine, 4.5 g/L glucose and 1% penicillin-streptomycin (PS) at 37°C in a 5% CO_2 incubator. For transient transfections, HEK293 cells were seeded onto 12 well plate (80000 cells per well) and cultured overnight. Transfection with 250 ng of control vector (pcDNA3) or overexpressing α-cardiac actin (p*Actc1*) constructs was carried out with the Lipofectamine 2000 transfection reagent (ThermoFisher, France), according to outlined protocol. After 48 hours of transfection, cells were changed to PS-free medium for 30 min at 37°C and washed with a solution of phosphate buffer solution (PBS). Then, cells were treated with 250 µM H_2O_2 for 60 min at 37°C. For control cells, this step was replaced by a PBS solution. Then the medium was changed by a DMEM medium containing 10% FBS, 2 mM glutamine and 1% PS and cells were cultured for 24 hours before experiments.

Statistical analyses

All the results were expressed as means ± s.e.m. For the echocardiographic and biomolecular data, the significance of differences between means was assessed with both Student's *t*-test and Mann-Whitney's test for nongaussian data. *P*-value of < 0.05 was considered to be statistically significant.

Results

1. Forced cardiac expression of α-cardiac actin preserves actin dynamics.

The first step of our study was to generate TGCA mice allowing cardio-specific tamoxifen-inducible overexpression of Actc1. We selected the line with the highest induction of the transgene close to 2.4 folds the endogenous level of Actc1 transcript level at 30 days after tamoxifen (Fig. S1E). At the protein level, there was no detectable change in α-cardiac actin level presumably due to the already high expression of the protein at baseline. The induction of Actc1 did not alter cardiac structure or function in TGCA mice (Fig. S1).

Breeding the TGCA mice with *Sf/Sf* mice then with SRF ^{HKO} mice generated SRF ^{HKO}/CA mice in which Actc1 rescue in the heart was induced at the same time when SRF was knock-out by tamoxifen injections (Fig. 1). We quantified the amount of *Actc1* mRNA by RT-qPCR in control, SRF ^{HKO} and SRF ^{HKO}/CA mice. We found that total *Actc1* mRNA level was rescued in SRF ^{HKO}/CA to 80% of the control group level at 30 days after tamoxifen (Fig. 2, A and B). These data were confirmed by Western blot analysis and showed an α-cardiac actin amount in the SRF ^{HKO}/CA group closer to the control group while a decrease of 50% was detected in the SRF ^{HKO} group (Fig. 2, C and D). SRF protein level was decreased by 80% in the SRF ^{HKO} and SRF ^{HKO}/CA group, as well, compared with the control group indicating that the disruption of SRF gene was similar in these two groups of mice (Fig. 2, C and D). We next determined the level of cardiac F-actin to G-actin. We showed that F/G actin ratio was significantly decreased in hearts of SRF ^{HKO} mice while it was partially maintained at 90% in hearts of SRF ^{HKO}/CA compared with control mice (100%) (Fig. 2, E and F).

2. Forced cardiac expression of α-cardiac actin maintains temporally cell cytoarchitecture.

Hearts of control, SRF ^{HKO} and rescued SRF ^{HKO}/CA mice were examined morphologically and histologically. Hematoxylin-eosin staining on heart sections shows an enlargement of the chambers and a decrease of ventricular wall thickness in SRF ^{HKO} mice at 45 days after tamoxifen injections whereas the cardiac chambers anatomy of SRF ^{HKO}/CA mice were similar to that of the control mice (Fig. 3A). These results were confirmed by evaluation of HW/BW ratio in the three groups of mice (4.85 ± 0.01 in control, 5.79 ± 0.02 in *SRF* ^{HKO} ($P <$ 0.001 versus control) and 5.25 ± 0.02 in SRF ^{HKO}*/CA* ($P <$ 0.05 versus control)) (Fig. 3B). Cardiac function was next assessed by echocardiography before (day 0) and 30 days after tamoxifen treatment. At day 0, similar values were observed for each group. At day 30 after

tamoxifen injections, the left ventricle free wall thickness at the end of the systole (LVFWs, 0.75 ± 0.02) and the ejection fraction (EF, 44.14 ± 2.38) were lower in the SRF ^{HKO} group while the SRF ^{HKO}/CA group showed an intermediate phenotype with a lesser decrease of LVFWs (0.85 ± 0.03) and EF (65.24 ± 3.71), closer to those obtained for control mice (LVFWs, 0.95 ± 0.03; EF, 82.03 ± 0.46) (Table 1). LV contractility parameters such as Vcfc, systolic velocity at mitral annulus (Sa) and posterior wall (Spw) were much better preserved in SRF ^{HKO}/CA mice compared with SRF ^{HKO} mice and only modestly affected compared with controls (Table 1). The left ventricular thickness to radius ratio was decreased only in SRF ^{HKO} group (h/r, 0.23 ± 0.01) but not in the SRF ^{HKO}/CA and control mice (0.30 ± 0.02, 0.31 ± 0.02, Table 1). E/Ea ratio, a diastolic LV parameter, remained identical in SRF ^{HKO}/CA mice (16.5 ± 0.5) to the ratio obtained for control mice (16.4 ± 0.6) while the increase of this ratio in SRF ^{HKO} mice (22.8 ± 0.8) suggests the occurrence of diastolic dysfunction in this latter group (Table 1). Cardiac cytoarchitecture was analyzed by confocal microscopy analysis after immunostaining for SRF and vinculin, a membrane-associated cytoskeletal protein (Fig. 3, C and D). No signal of SRF protein was detected in nuclei of cardiomyocytes of SRF ^{HKO} and of SRF ^{HKO}/CA mice compared with control mice (Fig. 3C). However, important structural and morphologic differences were observed between SRF ^{HKO} and SRF ^{HKO}/CA myocardium. SRF ^{HKO}/CA cardiomyocytes were homogeneous in size and their shape and alignment were regular without gaps between cells, although they remain negative for SRF (Fig. 3, C and D). In contrast**,** SRF ^{HKO} cardiomyocytes were stretched and heterogeneous in size and the intercalated discs were thick and dysmorphic as previously described (4, 14) (Fig. 3, C and D). The phalloidin staining for polymerized F-actin showed a better preservation of sarcomeric organization in SRF ^{HKO}/CA than in SRF ^{HKO} hearts (Fig. 3D). Morphometrical analysis revealed that SRF ^{HKO}/CA cardiomyocyte length and width distribution was closer to that of controls (Fig. 3E).

Electron microscopy of SRF ^{HKO}/CA heart at 35 days showed well-aligned arrays of myofibrils at the Z disks (Z) similar to that of control hearts whereas the myofibrils and Z disks are less dense in SRF ^{HKO} hearts (Fig. 4 A). Mitochondria alignment was preserved in SRF ^{HKO}/CA cardiomyocytes as in control whereas they were misaligned with an oval shape in SRF ^{HKO} group (Fig. 4A). In addition, the structure of intercalated disks in SRF ^{HKO}/CA and control hearts were thin and regular whereas this structure was altered in SRF ^{HKO} hearts (Fig**.** 4B).

3. Forced cardiac expression of α-cardiac actin corrected myocardial gene program.

The loss of SRF is known to lead to profound alterations of the cardiac gene expression program (4, 14, 18, 25-27). To investigate the impact of overexpression of α-cardiac actin on cardiac genomewide expression in SRF ^{HKO} hearts, we performed transcriptomic profiling of hearts from five groups of mice: 1) TGCRE expressing inducible Cre; 2) TGCA expressing rat α-cardiac actin transgene; 3) Srf-floxed Cre negative; 4) SRF ^{HKO} *and 5)* SRF ^{HKO}/CA mice. We analyzed each of the four groups of mice and compared them to a common control, homozygous *Srf-floxed; Cre* negative mice (Fig. 5A). All animals including controls, we subjected to the same protocol of tamoxifen injections.

We found that 2310 genes were differentially expressed in the hearts of SRF ^{HKO} group compared to control group, out of which 1536 genes (67%) at least 1.25-fold including 731 upregulated genes and 805 downregulated gene. By comparison, a total of 2.701 was differentially expressed in the heart of SRF ^{HKO}/CA mice, out of which 1820 genes (67%) at least 1.25-fold (806 up, 1.014 down). By comparison the TGCA modulated 1218 genes when overexpressed in wildtype background and the *TGCRE* that is required for *TGCA* induction and *Srf* gene deletion, hence common to all the groups except controls, modulated 1067 genes.

The Venn diagram analysis showed that the *TGCRE* may have a relatively small impact on the total set of differentially expressed genes in the 3 other groups. They were 212 genes in common with *TGCA*, 256 with SRF ^{HKO} (11% of differentially expressed genes in this group) and 322 with SRF ^{HKO}/CA (12% of differentially expressed genes in this group). Nevertheless, to increase the specificity of our GSEA analyses to the impact of the SRF deletion and/or TGCA expression in the heart, we removed those genes overlapping with the TGCRE from subsequent GSEA analyses to focus on the consequences of TGCA expression alone or in the SRF ^{HKO} background. TGCA overexpression alone modulated the expression of 726 genes involved in cytokine, actin cytoskeleton and tight junction signalling in a non-pathological background. These genes were not found in SRF ^{HKO}/CA showing that their modulation requires SRF activity. 275 genes modulated by TGCA were also modulated in SRF ^{HKO} group and 286 in the SRF ^{HKO}/CA with an overlap of 160 genes common to the 3 groups, suggesting that most of these genes are responsive to α-cardiac actin level perturbation independently of the presence of SRF. The SRF ^{HKO} and SRF ^{HKO}/CA hearts were the two conditions sharing the largest group of 966 common differentially expressed genes only in these two groups. Those genes were not changed by the rescue of α-cardiac actin and can therefore be considered as strictly SRF-dependent. Interestingly, a large group

of 901 differentially expressed genes in the SRF ^{HKO} hearts versus control were not significantly altered anymore in the SRF ^{HKO}/CA background. Those 901 genes represent 44 % of the 2053 SRF ^{HKO} differentially expressed genes (2310 - 257 TGCRE related genes) that could be considered as rescued to normal physiological level. The overexpression of α-cardiac actin in the SRF ^{HKO}/CA background resulted in a large set of 1226 differentially expressed genes that were not altered originally in the SRF ^{HKO} hearts nor were modulated by TGCA alone in a healthy cardiac context. This showed that α-cardiac actin rescue has a specific impact in the context of SRF ^{HKO} DCM phenotype.

Top canonical pathways enrichment revealed that oxidative phosphorylation (repressed) and purine nucleotides degradation (increased) are the two most affected pathways in the 901 genes that are differentially altered only in the SRF ^{HKO} hearts (Fig. S2). Although, mitochondrial dysfunction was still present in the 966 genes that were altered in common between SRF ^{HKO} and SRF ^{HKO}/CA hearts. However, when detailing the alteration of the oxidative phosphorylation pathway in each group compared to the control group, we observed that there were a lower number of repressed subunits of complex I, II and III of the electron transport chain (ETC) in the SRF ^{HKO}/CA hearts and a lower activation level of Complex IV subunits (Fig. 5B). On the other hand, α-cardiac actin rescue in the SRF ^{HKO}/CA hearts resulted in a specific increase in ATP5O gene encoding the ATP synthase peripheral stalk subunit ATP5O which improves the resistance to oxidative stress (28) (Fig. 5B). Altogether these differences suggest that the alteration of the ETC is less important in the context of α-cardiac actin rescue in the SRF ^{HKO}/CA hearts that could translate in lower ROS production.

Finally, α-cardiac actin overexpression specifically activated the actin nucleation pathway by ARP-WASP complex through an induction of integrin and Rho small G-protein signalling (Fig. 5C). It also activated the PI3K/AKT signalling which is known to be protective for the heart (Fig. 5D).

We completed the transcriptomic assay by performing RT-qPCR analyses. We first confirmed that SRF mRNA level was low in SRF ^{HKO} and in SRF ^{HKO}/CA, as well, compared with control group (Fig. S3). As previously shown (4), loss of SRF led to a decrease of mRNA level of skeletal α-actin, MCK and Serca2 (Fig. S3). The maintenance of α-cardiac actin expression did not improve the expression of these genes (Fig. S3). In the same way, a 22-fold increase of ANF mRNA level was detected in SRF ^{HKO} and SRF ^{HKO}/CA compared with control group (Fig. S3). Concerning myosin heavy chain (MHC) expression, the switch from predominant α- to β- isoforms that is associated to disease state in the SRF ^{HKO} hearts as in all models of heart failure did not occur when α-cardiac actin expression was maintained. In SRF

^{HKO}/CA mice, the level of postnatal cardiac fast αMHC mRNA was similar to the one observed in control mice and the increase of embryonic slow βMHC mRNAs was lower than in SRF ^{HKO} mice (Fig. S3). We also found that Myl4 and Myl7 mRNA levels, two embryonic myosin light chain isoforms, were increased in SRF ^{HKO} but maintained at a low level in SRF ^{HKO}/CA compared with control mice (Fig. S3). A profile almost similar was observed with the level of STARS transcripts, a gene involved in actin polymerization (Fig. S3). By Western blot analysis, we confirmed the data previously obtained by RT-qPCR analyses namely the expression of MCK and Serca2 proteins highly decreased and the expression of ANF increased in SRF ^{HKO} and in SRF ^{HKO}/CA compared with control mice (Fig. S4A). By electrophoretic separation, we precisely determined the α- and β- isoform expression of MHC protein. First, we showed a lower expression of the αMHC protein in SRF ^{HKO} mice (Fig. S4B). Undetectable in control mice, fetal cardiac βMHC protein is re-expressed in SRF ^{HKO} whereas this re-expression is attenuated in SRF ^{HKO}/CA mice (Fig. S4B). These data are in accordance with those of RT-qPCR analysis (Fig. S3).

4. Forced cardiac expression of α-cardiac actin improves DCM-associated oxidative stress.

Preservation of the mitochondrial electron transport chain which is the main source of reactive oxygen species and oxidative stress when dysfunctional, is one of the pathways improved by α-cardiac actin as indicated by the data obtained by the transcriptomic approach. Indeed, several studies have previously suggested a relationship between DCM pathogenesis and oxidative stress (29-31). Thus, we examined the impact of α-cardiac actin on the oxidative stress level in the heart by two approaches using DHE to detect superoxide production and DNA breaks in nuclei and carbonylated proteins by DNPH staining (Fig. 6). The higher DHE staining level was found in SRF ^{HKO} heart compared with a weak signal of control and SRF ^{HKO}/CA hearts (Fig. 6A). Little DHE signal was observed in nuclei from *SRF* ^{HKO}/CA and control hearts of mice while an intense signal was detected in a large number of cells in the SRF ^{HKO} hearts (Fig. 6A, white arrows). It has been known that oxidative stress leads to the addition of carbonyl groups (COO) that indiscriminately affects proteins (32, 33). Then, we analyzed the level of carbonylated proteins by DNPH staining on cardiac cross section (Fig. 6B) and by oxiblot strategy in our three groups of mice (Fig. 6, C and D). On SRF ^{HKO} cardiac cross section, DNPH carbonylation signal was strong compared with the signal obtained in SRF ^{HKO}/CA and control which was weakly detectable (Fig. 6B). These

data were supported by the oxiblot approach (Fig. 6, C and D).

5. Impact of α-cardiac actin on mitochondrial respiratory chain and NADPH oxidase enzymatic complex.

In heart, major sources of ROS production involve the mitochondrial respiratory chain and the NADPH oxidase enzymatic complex (NOX) mainly NOX2 and NOX4. To assess the impact of α-cardiac actin in these processes, we analyzed the expression of several specific genes in the hearts of the three groups of mice by RT-qPCR and Western blot analyses. We first quantified the expression of NOX2 and NOX4 genes. In SRF ^{HKO} mice, we showed a 3-fold and a 3.5-fold increase of NOX2 and NOX4 mRNA levels respectively whereas in SRF ^{HKO}/CA mice these levels were lower than those of the control mice (Fig. 7A). By Western blot analysis, we confirmed that NOX2 and NOX4 protein levels were high in SRF ^{HKO} mice while they remained low in SRF ^{HKO}/CA mice (Fig. 7B). Because Sirtuins (SIRT) play a particularly important role in the response to stress and toxicity, we examined the expression of SIRT1 (cytoplasmic and nuclear isoform) and SIRT3 (mitochondrial isoform). Triggering SRF loss led to a similar strong decrease in SIRT1 mRNA level irrespective of exogenous α-cardiac actin overexpression whereas SIRT3 mRNA level were unchanged compared with the control group (Fig. 7C). These data were confirmed for SIRT3 protein level by Western blot analysis (Fig. 7D). Interestingly, we evaluated the expression level of several proteins in isolated mitochondria. A 25% decrease of the Complex IV subunit protein level was observed in mitochondria of SRF ^{HKO} mice whereas this level was maintained closer to those of control in SRF ^{HKO}/CA mice (Fig. 7D). The levels of Aconitase2, SOD 2, and VDAC1 proteins were practically unaffected by SRF loss and by α-cardiac actin compensatory expression (Fig. 7D).

6. Protective effects against H_2O_2-induced oxidative stress by α-cardiac actin overexpression in cultured HEK293 cells.

To investigate the effects of α-cardiac actin on oxidative stress, we performed a set of transfection experiments in HEK293 cells that express β-actin and have a poorly developed cytoskeleton. Ectopic overexpression of α-cardiac actin was driven by a pcDNA3-plasmid containing the rat *Actc1* cDNA (*pActc1*). By Western blot analysis, we validated the expression of α-cardiac actin protein in transfected cells only (Fig. 8A). Then we performed a co-immunostaining for α-cardiac actin and phalloidin associated to F-actin. We showed that α-cardiac actin staining occurred specifically in p*Actc1*-transfected cells with a colocalization

between α-cardiac actin and polymerized F-actin suggesting that exogenous α-cardiac actin could participate in actin filament (Fig. 8B). The cells were exposed to H_2O_2 to assess the impact of α-cardiac actin (Fig. 8C). We performed a DHE staining coupled with α-cardiac actin immunostaining on pcDNA3 or p*Actc1*-transfected cells after H_2O_2 treatment. We observed that the cells overexpressing α-cardiac actin were protected against DNA break because less DHE signal was detected compared with control cells (pcDNA3 transfection) (Fig. 8C). DHE/DAPI ratio estimated by a double-blind counting showed a 3.25-fold increase in pcDNA3 cells exposed to H_2O_2 (Fig. 8D). By contrast, this ratio was similar between the H_2O_2 non-treated- and treated- p*Actc1*-transfected cells (Fig. 8D), indicating a protecting effect of *Actc1*.

Discussion

In adult mammalian heart, α-cardiac actin is a key component that is ideally placed to maintain the structural integrity of the myocardium not only at the cellular level but also at the tissue level by the virtue of its connection to cell-cell and cell-matrix interacting complexes (10-13). Nevertheless, its exact role in cardiac physiopathology remained hardly assessable. Our study was based on a transgenic strategy enabling a cardiac-specific transgenic *Actc1* compensatory expression in a mouse model of DCM based on SRF gene disruption in which *Actc1* is severely depressed. Our *in vivo* results demonstrated that maintenance of α-cardiac actin within cardiomyocytes temporally preserved cytoarchitecture from adverse cardiac remodelling through a positive impact on both structural and transcriptional aspects. Moreover, our main findings pointed out the protective effect of α-cardiac actin against deleterious oxidative stress during DCM development.

Previous studies on embryonic stem cells lacking SRF and on SRF ^{HKO} mouse model described a shift in actin equilibrium from F-actin toward G-actin and a decrease in overall actin concentration when SRF loss is triggered (4, 17, 34). In the heart of SRF ^{HKO}/CA mice, tamoxifen-induced activation of the *Actc1* transgene lead to preservation of both total α-cardiac actin expression level and notably F-actin pool. As previously described, DCM presented several features of cardiac cytoarchitecture alteration such as myofibrillar disorganization and a stretching of intercalated disks, leading to eccentric hypertrophy of cardiac cells. Here we showed that the presence of α-cardiac actin has major beneficial effects at cellular level. Despite the loss of SRF leading to the down-regulation of a number of

proteins belonging to the contractile apparatus cytoskeleton, cardiomyocytes expressing *Actc1* transgene conserved both their structural integrity and their cell-to-cell junctions. Thus, maintaining α-cardiac actin preserves these cells from contractile dysfunction and adverse remodelling process, hence delaying DCM development and functional defects.

Under pathological context, cardiomyocyte remodelling is associated with a disturbance of myocardial gene program (35, 36). Loss of SRF is rapidly followed by a drastic reduction of *Actc1* level such that it was difficult to know the specific effect of *Actc1* loss on other cardiac gene expression during DCM development (4, 14). Several studies have provided evidence for a significant role of actin in transcription and in chromatin remodelling. Actin is known to bind directly to all three classes of RNA polymerase and is required for their full transcriptional activity (37-39). In addition, actin participates in the recruitment of histone modifiers to transcribed genes by association with nascent messenger ribonucleoproteins (40, 41). In order to assess this transcriptional impact of α-cardiac actin, we used a whole genome microarray screening by affymetrix DNA chips. Following SRF loss, our bioinformatic analyses confirmed that close to 50% of genes that were altered in the SRF ^{HKO} remained altered when α-cardiac actin was rescued, which validated the crucial role of the SRF transcription factor upon cardiac muscle differentiation and function (22, 42-44). However, this also means that the rescue of a key structural protein, the α-cardiac actin, is sufficient to normalize a large fraction of cardiac genes. Apart from long-established SRF target genes, we also revealed gene families and specific pathways, which were specifically sensitive to α-cardiac actin level. Among the genes exhibiting the most significant difference, those involved in sarcomere contractility and oxidative stress regulation were overrepresented. Sarcomere contractility depends on few crucial parameters such as: 1- the relative ratio of α-cardiac to skeletal α-actin isoforms (11, 45, 46); 2 - the expression of actin polymerization factor like STARS/Abra (47); 3 - the imbalance between cardiac MHC isoforms which hold specific enzymatic and mechanical activities adjusted for whether *in utero* or post-natal force (48, 49). The switch from the predominant α-cardiac MHC rapid isoform with high ATPase activity in the healthy heart to the slow fetal β-cardiac MHC that has a slow contractile rate and low ATPase activity, is a typical feature of the failing heart. Our RT-qPCR and protein data validated that simply maintaining α-cardiac actin is sufficient to prevent the switch between adult and fetal myosin isoforms and the increase of STARS that is abnormally activated in the SRF ^{HKO} mutant as an attempt to maintain actin polymerization. Interestingly the α-skeletal actin gene, which is a direct target of SRF as α-cardiac actin, remains repressed in the SRF ^{HKO}/CA mice showing that there is no direct transcriptional cross-talk between the

two actin isoforms beside SRF. Taken together, our results confirmed the highly significant impact of α-cardiac actin on cardiac gene program and tended to suggest that this impact include several actin-associated proteins.

We hypothesized that α-cardiac actin could also play a role on the regulation of oxidative stress and production of ROS by restoring the mitochondrial integrity that is known to be sensitive to cytoskeleton perturbations. This was reflected at least in part by a less altered mitochondrial ETC. Oxidative stress is described as a leading cause of adverse cardiac remodelling, since it can interfere on myocardial contractile activity and function, propelling the severity of a large spectrum of cardiovascular disorders (50-52). We showed that preserving α-cardiac actin in the SRF ^{HKO} hearts lead to a reduction of DNA breaks and protein carbonylation that are usual features of deleterious oxidative stress. Further studies should address the identification of those specific proteins targeted by oxidation. In addition, our *in vitro* studies demonstrated that an ectopic expression of α-cardiac actin in HEK293 cells was enough to improve oxidative stress resistance in reducing both anion superoxide production and DNA breaks occurrence. This protective effect has been already described in budding yeast in which the capacity to survive elevated oxidative stress is sensitive to cytoplasmic actin dynamics though the exact process involved is still unknown (53, 54). Under pathological conditions, several sources of ROS lead to deleterious oxidative stress in the cardiac muscle, such as mitochondrial respiratory chain dysfunction and monooxygenase enzymes (55-58). So, is α-cardiac actin able to reduce oxidative stress by impacting on these sources of ROS? At first, we demonstrated that maintaining α-cardiac actin preserves the alignment of mitochondrial network and the global aspect of these organelles. In addition, a decrease of Complex IV subunit has been detected in the mitochondrial fraction of SRF ^{HKO} cardiac tissue but not in the heart of SRF ^{HKO}/CA mice, suggesting a clear difference concerning mitochondrial oxidative metabolism. A primary reduction of Complex IV could have secondary effects on the Complexes I, II and III by modification of the pool of mitochondrial electron transport chain leading them to a direct interaction of electrons with O^{2-} and an increase in the production of superoxide and subsequently of ROS. It has previously been established that ROS generation is located at the level of complexes I and III (59-62). Linked together, our findings argue to a better conservation of mitochondrial structure and function in cardiomyocytes maintaining Actc1 expression, F/G ratio and this could be associated with a more efficient ATP production. Mitochondrial potential and ATP import/export are channel dependent process. Voltage-dependent-anion channels (VDAC) represent a class of actin-dependent porins located on the outer mitochondrial membrane to

ensure the regulation of metabolic and energetic fluxes (63). It is well known that VDAC activity is regulated by actin, since actin depolymerization favours both channels opening and anionic release (6, 64). Although we did not detect significant modification of VDAC protein level, we can hypothesize that the difference of α-cardiac actin pool within sarcomeres could impact on VDAC activity in the cardiomyocytes of our different groups of mice. Produced by mitochondria but also by the pentose phosphate pathway, NADPH is a major cellular cofactor, which is mostly implicated in the redox imbalance as a powerful reducing agent. However, oxidation of NADPH catalysed by NOX complexes can also produce superoxide anion, initiating ROS production. NOX are composed of membrane, catalytic and cytosolic subunits that have to interact to ensure enzymatic activity (65, 66). It is known that NOX complex association is favoured by actin depolymerization in microglial Ra2 cell line (67, 68). Thus, we investigated whether α-cardiac actin could have an impact on NOX complex during DCM development. In our study, DCM development leads to an increase of NOX2 and NOX4 mRNA and protein levels when SRF loss is triggered. The impact of NOX2 and NOX4 activation on ROS production has been validated in both patients suffering from cardiac disease and rodent models of ischemia (69, 70). In cardiac cells, the increase of NOX levels did not occur when *Actc1* remained expressed. This is a major result and pointing out, for the first time, that α-cardiac actin level and organization could be involved in the regulation of NOX enzymes expression in cardiomyocytes. Although this regulation is still poorly understood, we suggest that this may be linked with sarcomere integrity and/or better subsarcolemal cytoskeleton preservation. Consequently, α-cardiac actin could preserve cardiomyocytes from exacerbated assembly of NOX complexes occurring when actin is less polymerized, thus reducing their heightened cytotoxic activity. Our findings lead us to suggest that α-cardiac actin could contribute to a healthy mitochondrial population within cardiomyocytes as well as to the global preservation of redox balance through a transcriptional impact on major redox enzymes.

In summary, our results revealed that α-cardiac actin plays a crucial role in cardiac function and integrity. It is able *per se* to preserve the structure of cardiomyocytes and to stabilize cardiac function despite a drastic SRF-triggering change of gene expression within myocardium. These data are relevant in a clinical context since α-cardiac actin is implicated in a growing number of cardiomyopathy or heart defect (9, 71, 72). Moreover, our *in vivo* and *in vitro* findings demonstrated that α-cardiac actin holds a protective effect against ROS massive production, preserving cardiomyocytes from several deleterious effects. Previous data validated the protective role of actin for oxidative stress survival in yeast (53, 54).

However, this is the first time that such a result has been demonstrated *in vivo in mammals*, and especially in cardiac muscle in which oxidative stress is a leading cause of adverse remodelling. This antioxidant impact of actin is notably linked with the preservation of both healthy mitochondrial population and low levels of NOX enzymes, two main potential sources of ROS. Finally, our study offers new therapeutic prospects for cardiac diseases by acting on α-cardiac actin level and polymerization state.

References

1. McNally, E. M., and Mestroni, L. (2017) Dilated Cardiomyopathy: Genetic Determinants and Mechanisms. *Circ Res* **121**, 731-748
2. Weintraub, R. G., Semsarian, C., and Macdonald, P. (2017) Dilated cardiomyopathy. *Lancet* **390**, 400-414
3. Codd, M. B., Sugrue, D. D., Gersh, B. J., and Melton, L. J., 3rd (1989) Epidemiology of idiopathic dilated and hypertrophic cardiomyopathy. A population-based study in Olmsted County, Minnesota, 1975-1984. *Circulation* **80**, 564-572
4. Parlakian, A., Charvet, C., Escoubet, B., Mericskay, M., Molkentin, J. D., Gary-Bobo, G., De Windt, L. J., Ludosky, M. A., Paulin, D., Daegelen, D., Tuil, D., and Li, Z. (2005) Temporally controlled onset of dilated cardiomyopathy through disruption of the SRF gene in adult heart. *Circulation* **112**, 2930-2939
5. Bui, A. L., Horwich, T. B., and Fonarow, G. C. (2011) Epidemiology and risk profile of heart failure. *Nature reviews. Cardiology* **8**, 30-41
6. Xu, Q., Dewey, S., Nguyen, S., and Gomes, A. V. (2010) Malignant and benign mutations in familial cardiomyopathies: insights into mutations linked to complex cardiovascular phenotypes. *J Mol Cell Cardiol* **48**, 899-909
7. Daehmlow, S., Erdmann, J., Knueppel, T., Gille, C., Froemmel, C., Hummel, M., Hetzer, R., and Regitz-Zagrosek, V. (2002) Novel mutations in sarcomeric protein genes in dilated cardiomyopathy. *Biochem Biophys Res Commun* **298**, 116-120
8. Mundia, M. M., Demers, R. W., Chow, M. L., Perieteanu, A. A., and Dawson, J. F. (2012) Subdomain location of mutations in cardiac actin correlate with type of functional change. *PLoS One* **7**, e36821
9. Olson, T. M., Michels, V. V., Thibodeau, S. N., Tai, Y. S., and Keating, M. T. (1998) Actin mutations in dilated cardiomyopathy, a heritable form of heart failure. *Science* **280**, 750-752

10. Sassoon, D. A., Garner, I., and Buckingham, M. (1988) Transcripts of alpha-cardiac and alpha-skeletal actins are early markers for myogenesis in the mouse embryo. *Development* **104**, 155-164
11. Suurmeijer, A. J., Clement, S., Francesconi, A., Bocchi, L., Angelini, A., Van Veldhuisen, D. J., Spagnoli, L. G., Gabbiani, G., and Orlandi, A. (2003) Alpha-actin isoform distribution in normal and failing human heart: a morphological, morphometric, and biochemical study. *J Pathol* **199**, 387-397
12. Vandekerckhove, J., Bugaisky, G., and Buckingham, M. (1986) Simultaneous expression of skeletal muscle and heart actin proteins in various striated muscle tissues and cells. A quantitative determination of the two actin isoforms. *J Biol Chem* **261**, 1838-1843
13. Kumar, A., Crawford, K., Close, L., Madison, M., Lorenz, J., Doetschman, T., Pawlowski, S., Duffy, J., Neumann, J., Robbins, J., Boivin, G. P., O'Toole, B. A., and Lessard, J. L. (1997) Rescue of cardiac alpha-actin-deficient mice by enteric smooth muscle gamma-actin. *Proc Natl Acad Sci U S A* **94**, 4406-4411
14. Touvron, M., Escoubet, B., Mericskay, M., Angelini, A., Lamotte, L., Santini, M. P., Rosenthal, N., Daegelen, D., Tuil, D., and Decaux, J. F. (2012) Locally expressed IGF1 propeptide improves mouse heart function in induced dilated cardiomyopathy by blocking myocardial fibrosis and SRF-dependent CTGF induction. *Dis Model Mech* **5**, 481-491
15. Sun, Q., Chen, G., Streb, J. W., Long, X., Yang, Y., Stoeckert, C. J., Jr., and Miano, J. M. (2006) Defining the mammalian CArGome. *Genome Res* **16**, 197-207
16. Minty, A., and Kedes, L. (1986) Upstream regions of the human cardiac actin gene that modulate its transcription in muscle cells: presence of an evolutionarily conserved repeated motif. *Mol Cell Biol* **6**, 2125-2136
17. Diguet, N., Mallat, Y., Ladouce, R., Clodic, G., Prola, A., Tritsch, E., Blanc, J., Larcher, J. C., Delcayre, C., Samuel, J. L., Friguet, B., Bolbach, G., Li, Z., and Mericskay, M. (2011) Muscle creatine kinase deficiency triggers both actin depolymerization and desmin disorganization by advanced glycation end products in dilated cardiomyopathy. *J Biol Chem* **286**, 35007-35019
18. Diguet, N., Trammell, S. A. J., Tannous, C., Deloux, R., Piquereau, J., Mougenot, N., Gouge, A., Gressette, M., Manoury, B., Blanc, J., Breton, M., Decaux, J. F., Lavery, G. G., Baczko, I., Zoll, J., Garnier, A., Li, Z., Brenner, C., and Mericskay, M. (2018) Nicotinamide Riboside Preserves Cardiac Function in a Mouse Model of Dilated

Cardiomyopathy. *Circulation* **137**, 2256-2273

19. Agbulut, O., Li, Z., Perie, S., Ludosky, M. A., Paulin, D., Cartaud, J., and Butler-Browne, G. (2001) Lack of desmin results in abortive muscle regeneration and modifications in synaptic structure. *Cell Motil Cytoskeleton* **49**, 51-66
20. Guillet-Deniau, I., Mieulet, V., Le Lay, S., Achouri, Y., Carre, D., Girard, J., Foufelle, F., and Ferre, P. (2002) Sterol regulatory element binding protein-1c expression and action in rat muscles: insulin-like effects on the control of glycolytic and lipogenic enzymes and UCP3 gene expression. *Diabetes* **51**, 1722-1728
21. Bradford, M. M. (1976) A rapid and sensitive method for the quantitation of microgram quantities of protein utilizing the principle of protein-dye binding. *Analytical biochemistry* **72**, 248-254
22. Parlakian, A., Tuil, D., Hamard, G., Tavernier, G., Hentzen, D., Concordet, J. P., Paulin, D., Li, Z., and Daegelen, D. (2004) Targeted inactivation of serum response factor in the developing heart results in myocardial defects and embryonic lethality. *Mol. Cell. Biol.* **24**, 5281-5289
23. Agbulut, O., Li, Z., Mouly, V., and Butler-Browne, G. S. (1996) Analysis of skeletal and cardiac muscle from desmin knock-out and normal mice by high resolution separation of myosin heavy-chain isoforms. *Biol Cell* **88**, 131-135
24. Blum, H., Beier, H., and Gross, H. J. (1987) Improved silver staining of plant proteins, RNA and DNA in polyacrylamide gels. *Electrophoresis* **8**, 93-99
25. Angelini, A., Li, Z., Mericskay, M., and Decaux, J. F. (2015) Regulation of Connective Tissue Growth Factor and Cardiac Fibrosis by an SRF/MicroRNA-133a Axis. *PLoS One* **10**, e0139858
26. Gary-Bobo, G., Parlakian, A., Escoubet, B., Franco, C. A., Clement, S., Bruneval, P., Tuil, D., Daegelen, D., Paulin, D., Li, Z., and Mericskay, M. (2008) Mosaic inactivation of the serum response factor gene in the myocardium induces focal lesions and heart failure. *Eur J Heart Fail* **10**, 635-645
27. Tritsch, E., Mallat, Y., Lefebvre, F., Diguet, N., Escoubet, B., Blanc, J., De Windt, L. J., Catalucci, D., Vandecasteele, G., Li, Z., and Mericskay, M. (2013) An SRF/miR-1 axis regulates NCX1 and annexin A5 protein levels in the normal and failing heart. *Cardiovasc Res* **98**, 372-380
28. Wu, Y. T., Lee, H. C., Liao, C. C., and Wei, Y. H. (2013) Regulation of mitochondrial F(o)F(1)ATPase activity by Sirt3-catalyzed deacetylation and its deficiency in human cells harboring 4977bp deletion of mitochondrial DNA. *Biochim Biophys Acta* **1832**,

216-227

29. Dieterich, S., Bieligk, U., Beulich, K., Hasenfuss, G., and Prestle, J. (2000) Gene expression of antioxidative enzymes in the human heart: increased expression of catalase in the end-stage failing heart. *Circulation* **101**, 33-39
30. Ide, T., Tsutsui, H., Kinugawa, S., Suematsu, N., Hayashidani, S., Ichikawa, K., Utsumi, H., Machida, Y., Egashira, K., and Takeshita, A. (2000) Direct evidence for increased hydroxyl radicals originating from superoxide in the failing myocardium. *Circ Res* **86**, 152-157
31. Lynch, T. L. t., Sivaguru, M., Velayutham, M., Cardounel, A. J., Michels, M., Barefield, D., Govindan, S., dos Remedios, C., van der Velden, J., and Sadayappan, S. (2015) Oxidative Stress in Dilated Cardiomyopathy Caused by MYBPC3 Mutation. *Oxid Med Cell Longev* **2015**, 424751
32. Dalle-Donne, I., Giustarini, D., Colombo, R., Rossi, R., and Milzani, A. (2003) Protein carbonylation in human diseases. *Trends Mol Med* **9**, 169-176
33. Dalle-Donne, I., Rossi, R., Giustarini, D., Milzani, A., and Colombo, R. (2003) Protein carbonyl groups as biomarkers of oxidative stress. *Clin Chim Acta;* **329**, 23-38
34. Schratt, G., Philippar, U., Berger, J., Schwarz, H., Heidenreich, O., and Nordheim, A. (2002) Serum response factor is crucial for actin cytoskeletal organization and focal adhesion assembly in embryonic stem cells. *J Cell Biol* **156**, 737-750
35. Asakura, M., and Kitakaze, M. (2009) Global gene expression profiling in the failing myocardium. *Circ J* **73**, 1568-1576
36. Harvey, P. A., and Leinwand, L. A. (2011) The cell biology of disease: cellular mechanisms of cardiomyopathy. *J Cell Biol* **194**, 355-365
37. Hofmann, W. A., Stojiljkovic, L., Fuchsova, B., Vargas, G. M., Mavrommatis, E., Philimonenko, V., Kysela, K., Goodrich, J. A., Lessard, J. L., Hope, T. J., Hozak, P., and de Lanerolle, P. (2004) Actin is part of pre-initiation complexes and is necessary for transcription by RNA polymerase II. *Nat Cell Biol* **6**, 1094-1101
38. Hu, P., Wu, S., and Hernandez, N. (2004) A role for beta-actin in RNA polymerase III transcription. *Genes Dev* **18**, 3010-3015
39. Philimonenko, V. V., Zhao, J., Iben, S., Dingova, H., Kysela, K., Kahle, M., Zentgraf, H., Hofmann, W. A., de Lanerolle, P., Hozak, P., and Grummt, I. (2004) Nuclear actin and myosin I are required for RNA polymerase I transcription. *Nat Cell Biol* **6**, 1165-1172
40. Percipalle, P., Jonsson, A., Nashchekin, D., Karlsson, C., Bergman, T., Guialis, A.,

and Daneholt, B. (2002) Nuclear actin is associated with a specific subset of hnRNP A/B-type proteins. *Nucleic Acids Res* **30**, 1725-1734

41. Sjolinder, M., Bjork, P., Soderberg, E., Sabri, N., Farrants, A. K., and Visa, N. (2005) The growing pre-mRNA recruits actin and chromatin-modifying factors to transcriptionally active genes. *Genes Dev* **19**, 1871-1884
42. Kuwahara, K., Teg Pipes, G. C., McAnally, J., Richardson, J. A., Hill, J. A., Bassel-Duby, R., and Olson, E. N. (2007) Modulation of adverse cardiac remodeling by STARS, a mediator of MEF2 signaling and SRF activity. *J Clin Invest* **117**, 1324-1334
43. Miano, J. M., Ramanan, N., Georger, M. A., de Mesy Bentley, K. L., Emerson, R. L., Balza, R. O., Jr., Xiao, Q., Weiler, H., Ginty, D. D., and Misra, R. P. (2004) Restricted inactivation of serum response factor to the cardiovascular system. *Proc Natl Acad Sci U S A* **101**, 17132-17137
44. Zhang, X., Azhar, G., Chai, J., Sheridan, P., Nagano, K., Brown, T., Yang, J., Khrapko, K., Borras, A. M., Lawitts, J., Misra, R. P., and Wei, J. Y. (2001) Cardiomyopathy in transgenic mice with cardiac-specific overexpression of serum response factor. *Am. J. Physiol. Heart Circ. Physiol.* **280**, H1782-H1792
45. Garner, I., Minty, A. J., Alonso, S., Barton, P. J., and Buckingham, M. E. (1986) A 5' duplication of the alpha-cardiac actin gene in BALB/c mice is associated with abnormal levels of alpha-cardiac and alpha-skeletal actin mRNAs in adult cardiac tissue. *EMBO J* **5**, 2559-2567
46. Hewett, T. E., Grupp, I. L., Grupp, G., and Robbins, J. (1994) Alpha-skeletal actin is associated with increased contractility in the mouse heart. *Circ Res* **74**, 740-746
47. Lamon, S., Wallace, M. A., and Russell, A. P. (2014) The STARS signaling pathway: a key regulator of skeletal muscle function. *Pflug Arch Eur J Phy* **466**, 1659-1671
48. de Tombe, P. P. (2003) Cardiac myofilaments: mechanics and regulation. *J Biomech* **36**, 721-730
49. Suzuki, M., Fujita, H., and Ishiwata, S. (2005) A new muscle contractile system composed of a thick filament lattice and a single actin filament. *Biophys J* **89**, 321-328
50. Halliwell, B., and Cross, C. E. (1994) Oxygen-derived species: their relation to human disease and environmental stress. *Environ Health Perspect* **102 Suppl 10**, 5-12
51. Shao, D., Oka, S., Brady, C. D., Haendeler, J., Eaton, P., and Sadoshima, J. (2012) Redox modification of cell signaling in the cardiovascular system. *J Mol Cell Cardiol* **52**, 550-558

52. Victorino, V. J., Mencalha, A. L., and Panis, C. (2015) Post-translational modifications disclose a dual role for redox stress in cardiovascular pathophysiology. *Life Sci* **129**, 42-47
53. Farah, M. E., and Amberg, D. C. (2007) Conserved actin cysteine residues are oxidative stress sensors that can regulate cell death in yeast. *Mol Biol Cell* **18**, 1359-1365
54. Farah, M. E., Sirotkin, V., Haarer, B., Kakhniashvili, D., and Amberg, D. C. (2011) Diverse protective roles of the actin cytoskeleton during oxidative stress. *Cytoskeleton* **68**, 340-354
55. Bedard, K., and Krause, K. H. (2007) The NOX family of ROS-generating NADPH oxidases: physiology and pathophysiology. *Physiol Rev* **87**, 245-313
56. Ichihara, S., Suzuki, Y., Chang, J., Kuzuya, K., Inoue, C., Kitamura, Y., and Oikawa, S. (2017) Involvement of oxidative modification of proteins related to ATP synthesis in the left ventricles of hamsters with cardiomyopathy. *Sci Rep* **7**, 9243
57. Nabeebaccus, A., Zhang, M., and Shah, A. M. (2011) NADPH oxidases and cardiac remodelling. *Heart Fail Rev* **16**, 5-12
58. Paravicini, T. M., and Touyz, R. M. (2008) NADPH oxidases, reactive oxygen species, and hypertension: clinical implications and therapeutic possibilities. *Diabetes Care* **31 Suppl 2**, S170-180
59. Chen, Q., Vazquez, E. J., Moghaddas, S., Hoppel, C. L., and Lesnefsky, E. J. (2003) Production of reactive oxygen species by mitochondria: central role of complex III. *J Biol Chem* **278**, 36027-36031
60. Han, D., Antunes, F., Canali, R., Rettori, D., and Cadenas, E. (2003) Voltage-dependent anion channels control the release of the superoxide anion from mitochondria to cytosol. *J Biol Chem* **278**, 5557-5563
61. St-Pierre, J., Buckingham, J. A., Roebuck, S. J., and Brand, M. D. (2002) Topology of superoxide production from different sites in the mitochondrial electron transport chain. *J Biol Chem* **277**, 44784-44790
62. Turrens, J. F. (2003) Mitochondrial formation of reactive oxygen species. *J Physiol* **552**, 335-344
63. Shoshan-Barmatz, V., De Pinto, V., Zweckstetter, M., Raviv, Z., Keinan, N., and Arbel, N. (2010) VDAC, a multi-functional mitochondrial protein regulating cell life and death. *Mol Aspects Med* **31**, 227-285
64. Gourlay, C. W., and Ayscough, K. R. (2005) Identification of an upstream regulatory

pathway controlling actin-mediated apoptosis in yeast. *J Cell Sci* **118**, 2119-2132

65. Nauseef, W. M. (2008) Biological roles for the NOX family NADPH oxidases. *J Biol Chem* **283**, 16961-16965
66. Vignais, P. V. (2002) The superoxide-generating NADPH oxidase: structural aspects and activation mechanism. *Cell Mol Life Sci* **59**, 1428-1459
67. Paclet, M. H., Berthier, S., Kuhn, L., Garin, J., and Morel, F. (2007) Regulation of phagocyte NADPH oxidase activity: identification of two cytochrome b558 activation states. *FASEB J* **21**, 1244-1255
68. Rasmussen, I., Pedersen, L. H., Byg, L., Suzuki, K., Sumimoto, H., and Vilhardt, F. (2010) Effects of F/G-actin ratio and actin turn-over rate on NADPH oxidase activity in microglia. *BMC Immunol* **11**, 44
69. Cave, A., Grieve, D., Johar, S., Zhang, M., and Shah, A. M. (2005) NADPH oxidase-derived reactive oxygen species in cardiac pathophysiology. *Philos Trans R Soc Lond B Biol Sci* **360**, 2327-2334
70. Tsutsui, H., Kinugawa, S., and Matsushima, S. (2011) Oxidative stress and heart failure. *Am J Physiol Heart Circ Physiol* **301**, H2181-2190
71. Debold, E. P., Saber, W., Cheema, Y., Bookwalter, C. S., Trybus, K. M., Warshaw, D. M., and Vanburen, P. (2010) Human actin mutations associated with hypertrophic and dilated cardiomyopathies demonstrate distinct thin filament regulatory properties in vitro. *J Mol Cell Cardiol* **48**, 286-292
72. Muller, M., Mazur, A. J., Behrmann, E., Diensthuber, R. P., Radke, M. B., Qu, Z., Littwitz, C., Raunser, S., Schoenenberger, C. A., Manstein, D. J., and Mannherz, H. G. (2012) Functional characterization of the human alpha-cardiac actin mutations Y166C and M305L involved in hypertrophic cardiomyopathy. *Cell Mol Life Sci* **69**, 3457-3479

Competing Interests

The authors declare that they do not have any competing or financial interests.

Funding

This work was supported by l'Association Française contre les Myopathies (AFM#19814). AA was supported by a PhD fellowship of Université Paris 05, a fellowship of Fondation de la Recherche Médicale (FRM) and a fellowship of Groupe de Reflexion sur la Recherche Cardiovasculaire (GRRC) and Société Française de Cardiologie (SFC).

Acknowledgements

We thank Prof. Denise Paulin, Dr. Ara Parlakian, Prof. Onnik Agbulut, Dr. Dominique Daegelen, Dr. Marie-Thérèse Daher and Dr. Jocelyne Blanc for fruitful discussions and technique assistance, the IBPS platform for confocal microscopy analysis (Paris, France). We also thank the Genom'IC and Animal Care core facilities of Cochin Institute (Paris, France).

Author contributions

J.-F.D., Z.L. and M.M. conceived and designed the experiments. J.-F.D. created the transgenic mouse line overexpressing α-cardiac actin. A.A., M.-A.G., F.D., N.M., M.C., A.M. and J.-F.D. performed the experiments. A.A., F.D., Z.L., M.M. and J.-F.D. contributed to data analysis. A.A., M.M., Z.L. and J.-F.D. wrote the manuscript.

Legends

Figure 1: Simultaneous inducible cardiac-specific SRF disruption and α-cardiac actin compensatory expression in adult mice.

Schematic representation of the genetic strategy used to obtain a cardiac-specific SRF disruption and α-cardiac actin compensatory expression in adult mice. Tamoxifen injections to the triple transgenic mice (αMHC-MerCreMer: loxP-CAT-loxP-CardAct : Sf/Sf) induce simultaneous excision of the floxed CAT and SRF genes that allows the expression of transgenic α-cardiac actin associated with SRF inactivation.

Figure 2: Characterization of α-cardiac actin compensatory expression and effects on F/G-actin ratio.

A: Representative gels stained for RT-qPCR products with primers common to endogenous and exogenous *Actc1* (upper panel) or specific for the transgenic *Actc1* (Tg-r-ACTC1) in the heart of the three groups of mice at 30 days after tamoxifen injection. 18S ribosomal gene was used as loading control. B: RT-qPCR analysis of control (n = 6), SRF ^{HKO} (n = 6) and SRF ^{HKO}/ACTC1 (n = 6) Actc1 mRNA. Data are presented as means ± s.e.m. *** indicates significant difference at $P < 0.001$ versus the control group and, $^{###}$ at $P < 0.001$ versus the SRF ^{HKO} group. C: Western blot analysis for SRF (57 and 67 kDa) and ACTC1 (42 kDa) proteins. The blot was probed with anti-GAPDH (37 kDa) as loading control. D: Quantification of SRF and ACTC1 proteins (n=4). Data are means ± s.e.m. * and ** indicate significant difference at $P < 0.05$ and $P < 0.01$ versus the control group and, $^{###}$ at $P < 0.001$ versus the SRF ^{HKO} group. E: Distribution of F/G actin ratio from cardiac tissues of the three groups of mice. Samples were prepared as described in Materials and Methods. F: Relative densitometry of F/G actin distribution (n=4). Data are means ± s.e.m. * and ** indicate significant difference at $P < 0.05$ and $P < 0.01$ versus the control group and, $^{#}$ at $P < 0.05$ versus the SRF ^{HKO} group. ACTC1: α-cardiac actin; GAPDH: glyceraldehyde-3-phosphate transferase; G: globular actin; F : filamentous actin.

Figure 3: Impact of α-cardiac actin compensatory expression on DCM development and cardiomyocyte cytoarchitecture.

A: Hematoxylin-eosin staining of heart sections from control, SRF ^{HKO} and SRF ^{HKO}/CA mice at 45 days after tamoxifen injection. Data are representative of four independent experiments. RV: right ventricle; LV: left ventricle. Scale bar: 1 mm. B: HW/BW ratio measured in the three groups of mice (19 per group). Data are means ± s.e.m. * and *** indicate significant difference at $P < 0.05$ and $P < 0.001$ versus the control group and, $^{###}$ at $P < 0.001$ versus the SRF ^{HKO} group. HW: heart weight; BW: body weight. C: Confocal microscopy of cardiac sections labeled with anti-SRF antibody (red) and with anti-vinculin (green). Note that nuclear SRF expression was just observed in cardiomyocytes of control mouse (orange arrow). These results are representative of four separated experiments. Scale bar: 20 µm. D: Confocal microscopy of cardiac sections labeled with F-actin phalloidin staining (red) and anti-vinculin FITC (green). Compared with SRF ^{HKO} group, intercalated disks (white arrows) of SRF ^{HKO}/CA are thin, regular and closer to control group. Data are representative of three separated experiments. Scale bar: 20 µm. E: Distribution of cardiomyocyte lengths and widths

in the different groups of mice. Data are means ± SEM for 200 cardiomyocytes for each group of mice, including three different mice per group. Data are means ± s.e.m. *, ** and *** indicate significant difference at $P < 0.05$, $P < 0.01$ and $P < 0.001$ versus the control group and, $^{\#\#}$ and $^{\#\#\#}$ at $P < 0.01$ and $P < 0.001$ versus the SRF ^{HKO} group.

Figure 4: Transmission electronic microscopy from cardiac muscle of control, SRF ^{HKO} and SRF ^{HKO}/CA mice.

A: Sarcomere structure of cardiomyocytes. The SRF ^{HKO}/CA hearts have well-aligned arrays of myofibrils at Z disks (Z) and M line (M) as control whereas the myofibrils and Z disks are disrupted in SRF ^{HKO} hearts. Mitochondria (Mt) alignment is clearly preserved in SRF ^{HKO}/CA whereas they are flattened in SRF ^{HKO} hearts. B: Visualization of intercalated disks by red arrows. The structure of intercalated disks was altered in SRF ^{HKO} hearts with extensive interdigitation compared with SRF ^{HKO}/CA and control hearts. Experiments were done 35 days after tamoxifen treatment. Data are representative of two separated experiments. Scale bar: 1 µm.

Figure 5: Ingenuity Pathway Analyses (IPA) for top canonical pathways differentially enriched in SRF ^{HKO} and SRF ^{HKO}/CA using differentially expressed genes in hearts.

A: Venn diagram analysis of differentially expressed genes in the heart of *TGCA* mice, *TGCRE* mice, SRF ^{HKO} mice and rescued SRF ^{HKO}/CA mice. B: The mitochondrial oxidative phosphorylation pathway is severely affected in the SRF ^{HKO} hearts. Interestingly, although still perturbated in the SRF ^{HKO}/CA heart, there are less Complex I, II and III subunits affected than in the SRF ^{HKO} context, as well as lower increase in Complex IV subunits, and stimulation of ATP synthase peripheral stalk subunit ATP5O. C: The actin nucleation by ARP-WASP complex pathway specific to SRF ^{HKO}/CA (1226 genes). Activation of the actin nucleation pathway by ARP-WASP complex through an induction of integrin and Rho small G-protein signalling was observed when α-cardiac actin overexpressed in SRF ^{HKO} background. D: The PIA3K/AKT signaling pathway specific to SRF ^{HKO}/CA. Activation the PI3K/AKT signalling which is known to be cardio-protective was observed in SRF ^{HKO}/CA hearts.

TGCRE= α-MHC-MerCreMer transgene; *TGCA*=CAG-Actc1: α-MHC-MerCreMer transgene. Red color background indicated the up-regulation and inversely green color background the down-regulation.

Figure 6: DCM-associated deleterious oxidative stress is reduced by transgenic α-cardiac actin supply.

A: Superoxyde production and DNA breaks detection by dihydroethidium (DHE, red), staining of nuclei by DAPI (blue) and vinculin immunostaining (green) on cardiac sections. The white arrows indicate the colocalization between DHE and DAPI in nuclei of cardiac cells. Data are representative of four independent experiments. Scale bar: 20 µm. B: Detection of carbonylated proteins by Dinitrophenylhydrazin (DNPH, red) on cardiac sections. DNPH carbonylation signal is elevated in SRF ^{HKO} compared with control and SRF ^{HKO}*/CA* heart sections. Data are representative of 3 independent experiments. Scale bar: 60 µm. C: Oxiblot analysis. Carbonylated protein was detected using Hydrazin-Cy5 on SDS-PAGE (15 µg of proteins per well). Data are representative of four independent experiments. D: Quantification of carbonylated protein from Oxiblot experiments. Data are means ± s.e.m. ** and *** indicate significant difference at $P < 0.01$ and $P < 0.001$ versus the control group and, $^{\#\#}$ at $P < 0.01$ versus the SRF ^{HKO} group.

Figure 7: Impact of α-cardiac actin overexpression on the oxidative stress profile.

A: RT-qPCR analysis of mRNA of NOX2 and NOX4 genes in control (n=8), SRF ^{HKO} (n=8) and SRF ^{HKO}/CA (n=8) mouse hearts. Data are means ± s.e.m. * and ** indicate significant difference at $P < 0.05$ and $P < 0.01$ versus the control group and, $^{\#\#}$ and $^{\#\#\#}$ at $P < 0.01$ and $P < 0.001$ versus the SRF ^{HKO} group. B: Western blot analysis of NOX2 and NOX4 proteins (10 µg of total protein per lane), GAPDH protein was used as a loading control. C: RT-qPCR analysis of mRNA of SIRT1 and SIRT3 genes in control (n=8), SRF ^{HKO} (n=8) and SRF ^{HKO}/CA (n=8) mouse mRNA. Data are means ± s.e.m. * indicates significant difference at $P < 0.05$ versus the control group. D: Western blot analysis of VDAC1, C IV, SIRT3, SOD 2 and Aconitase2 proteins (10 µg of mitochondrial protein per lane), NDUFA9 protein was used as a loading control. These data are representative of three independent experiments.

Figure 8: A protective effects against H_2O_2-induced oxidative stress was observed by α-cardiac actin overexpression in HEK293 cells.

A: Western blot analysis of ACTC1 protein (20 µg of total proteins per lane) after 48 hours transfection of pActc1 plasmid overexpression in HEK293 cells. The cytoplasmic α-actin was used as loading control. These results are representative of three separated experiments. B: Immunofluorescent staining for F-actin by phalloidin (green), α-cardiac actin (red) and DAPI (blue) in HEK293 cells 48 hours after transfection of pcDNA3 (control) or pActc1 plasmids.

F-actin/ACTC1 signal colocalization is indicated by a white arrow. Scale bar: 20 µm. C: Immunofluorescent staining for α-cardiac actin (green) and DAPI (blue) in HEK293 cells 72 hours after transfection. Cells were transfected with pcDNA3 or pActc1 plasmids for 48 hours, treated by H_2O_2 250 µM for 60 min and then cultured for 24 hours. Detection of DNA breaks was done by dihydroethidium (red colour, white arrow). Scale bar: 15 µm. D: Quantitative analysis of DHE-positive to DAPI-stained nuclei ratio in HEK293 cells 72 hours after transfection, 200 were counted cells per experiment, n=3. Data are means ± s.e.m. *** indicate significant difference at $P < 0.001$ versus untreated cells (NT) for pcDNA3 and, ### at $P < 0.001$ versus transfected cells with pcDNA3 and treated by H_2O_2. NT: untreated cells.

Table 1: Functional phenotype in control, SRF ^{HKO} and SRF ^{HKO}/CA mice.

Echocardiographic measurements of control, SRF ^{HKO} and SRF ^{HKO}/CA mice at 0 and 30 days after tamoxifen treatment (n=9 mice per group). Data are presented as means ± s.e.m. [a] indicates significant difference at $P < 0.05$ versus the control group and, [b] significant difference at $P < 0.05$ between the SRF ^{HKO}/CA versus the SRF ^{HKO} group. BW: Body weight; HR: Heart rate; h/r: heart/radius ratio; LVFWs: Left Ventricle Free Wall systolic; LVFWd: Left Ventricle Free Wall diastolic; EF: Ejection Fraction; Vcfc: Shortening of velocity of circumferential fibers corrected for heart rate; Sa and Spw: Systolic velocity at mitral annulus and posterior wall, respectively; E/Ea: Ratio of transmitral blood velocity to mitral annulus diastolic velocity.

Figure 1

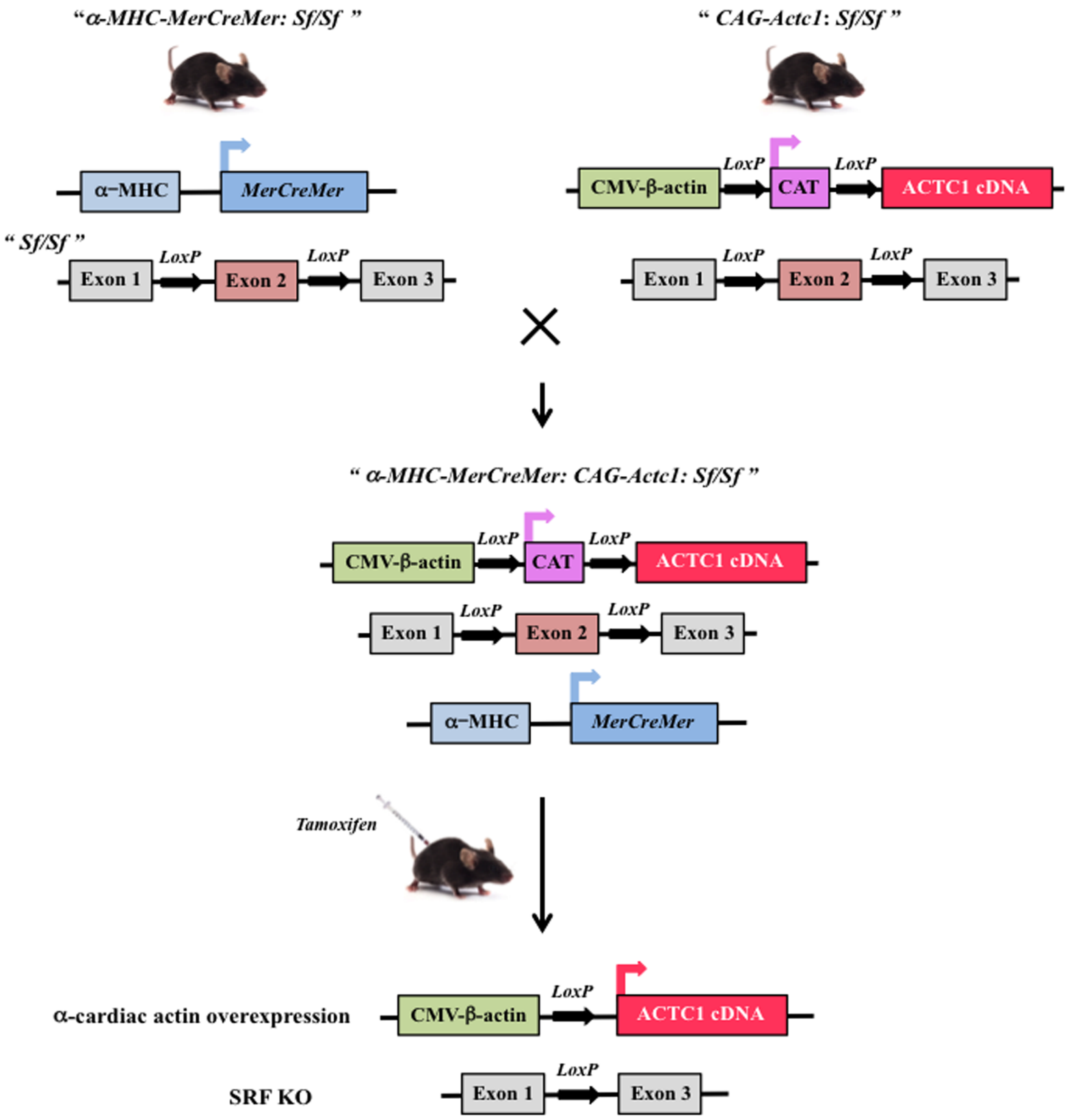
"α-MHC-MerCreMer: Sf/Sf "
" CAG-Actc1: Sf/Sf "
α−MHC
MerCreMer
CMV-β-actin
LoxP
CAT
ACTC1 cDNA
" Sf/Sf "
Exon 1
Exon 2
Exon 3
" α-MHC-MerCreMer: CAG-Actc1: Sf/Sf "
Tamoxifen
α-cardiac actin overexpression
SRF KO

Figure 2

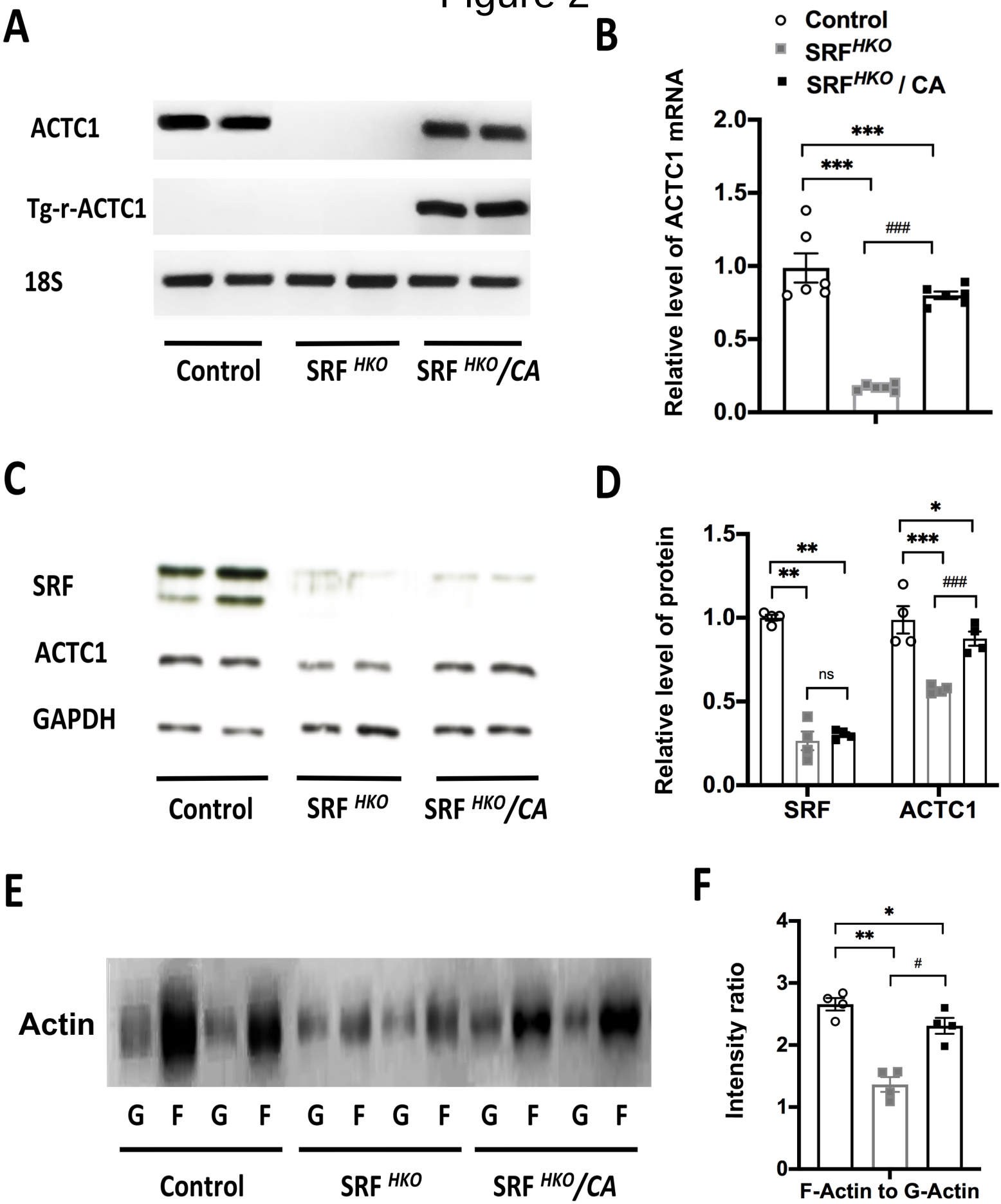
A
ACTC1
Tg-r-ACTC1
18S
Control
SRF HKO
SRF HKO/CA
B
Control
SRF HKO
SRF HKO / CA
Relative level of ACTC1 mRNA
2.0
1.5
1.0
0.5
0.0
***
***
###
C
SRF
ACTC1
GAPDH
Control
SRF HKO
SRF HKO/CA
D
Relative level of protein
1.5
1.0
0.5
0.0
**
**
ns
*
***
###
SRF
ACTC1
E
Actin
G F G F G F G F G F G F
Control
SRF HKO
SRF HKO/CA
F
Intensity ratio
4
3
2
1
0
*
**
#
F-Actin to G-Actin

Figure 3

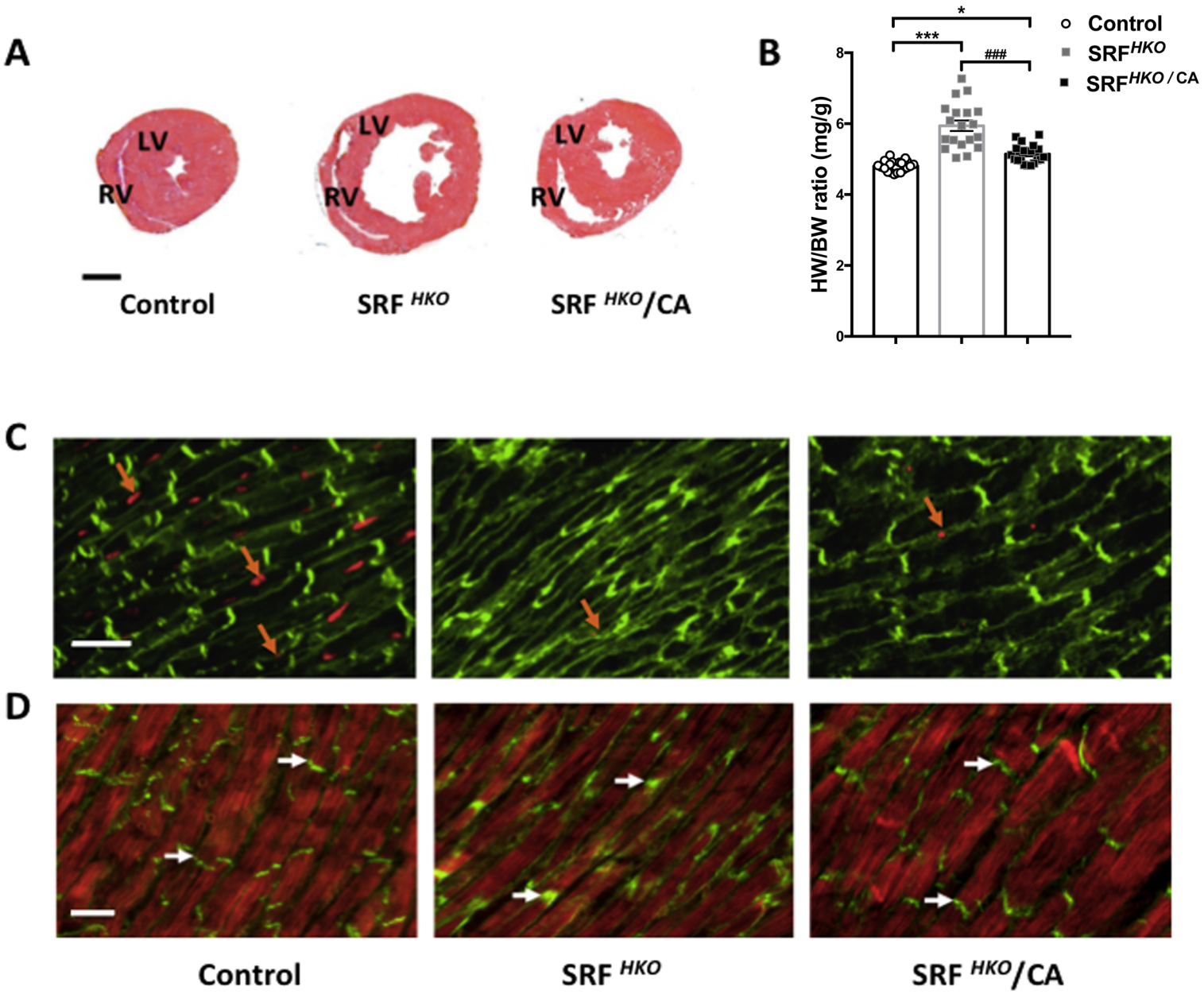
A
LV
RV
Control
SRF HKO
SRF HKO/CA
B
HW/BW ratio (mg/g)
Control
SRFHKO
SRFHKO / CA
C
D
Control
SRF HKO
SRF HKO/CA
E
Length (% of counted cells)
25<X< 50
51<X< 75
76<X
μm
Width (% of counted cells)
X<7,0
7.1<X<10
10,1<X
μm

Figure 4

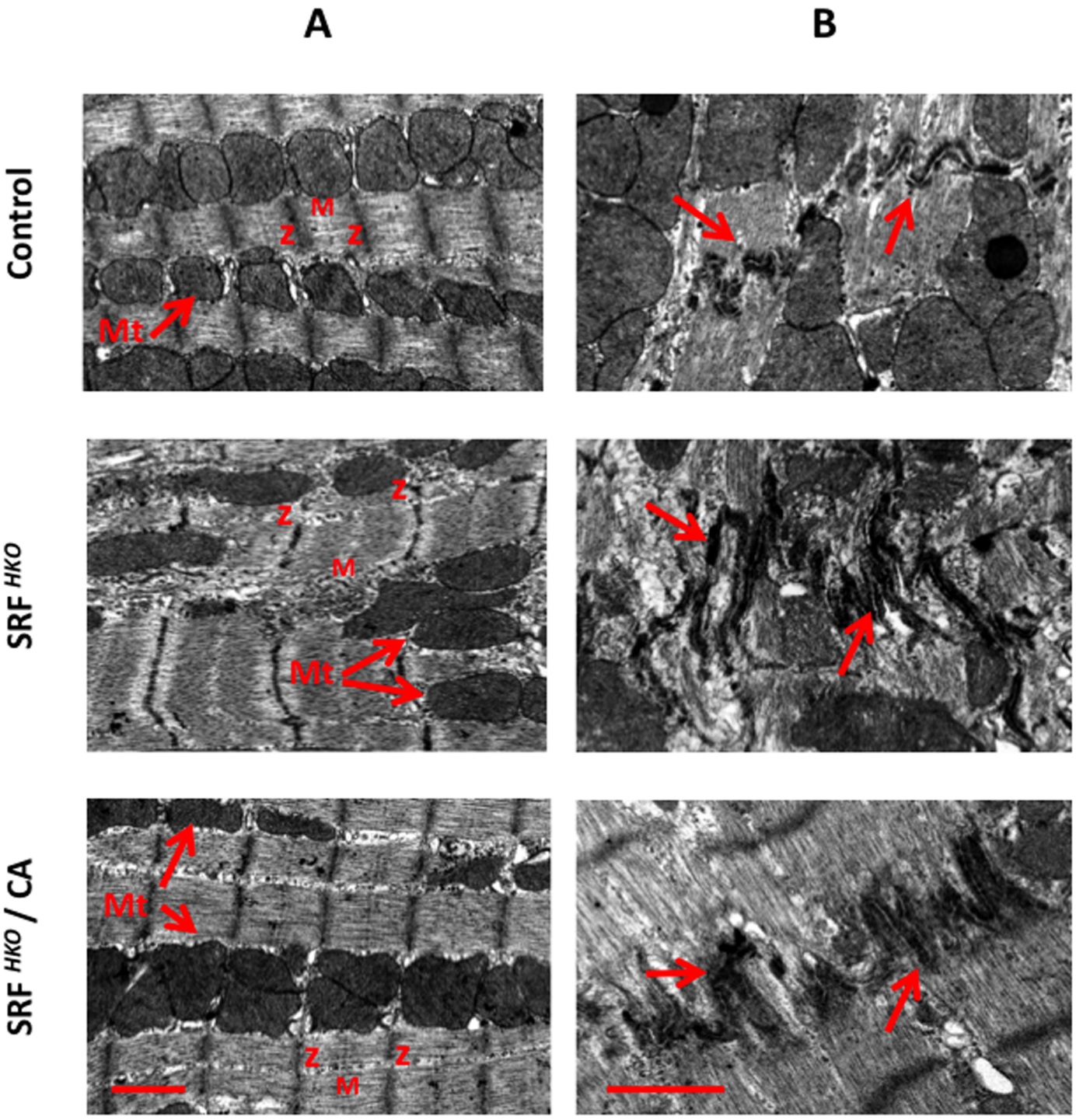

Figure 5

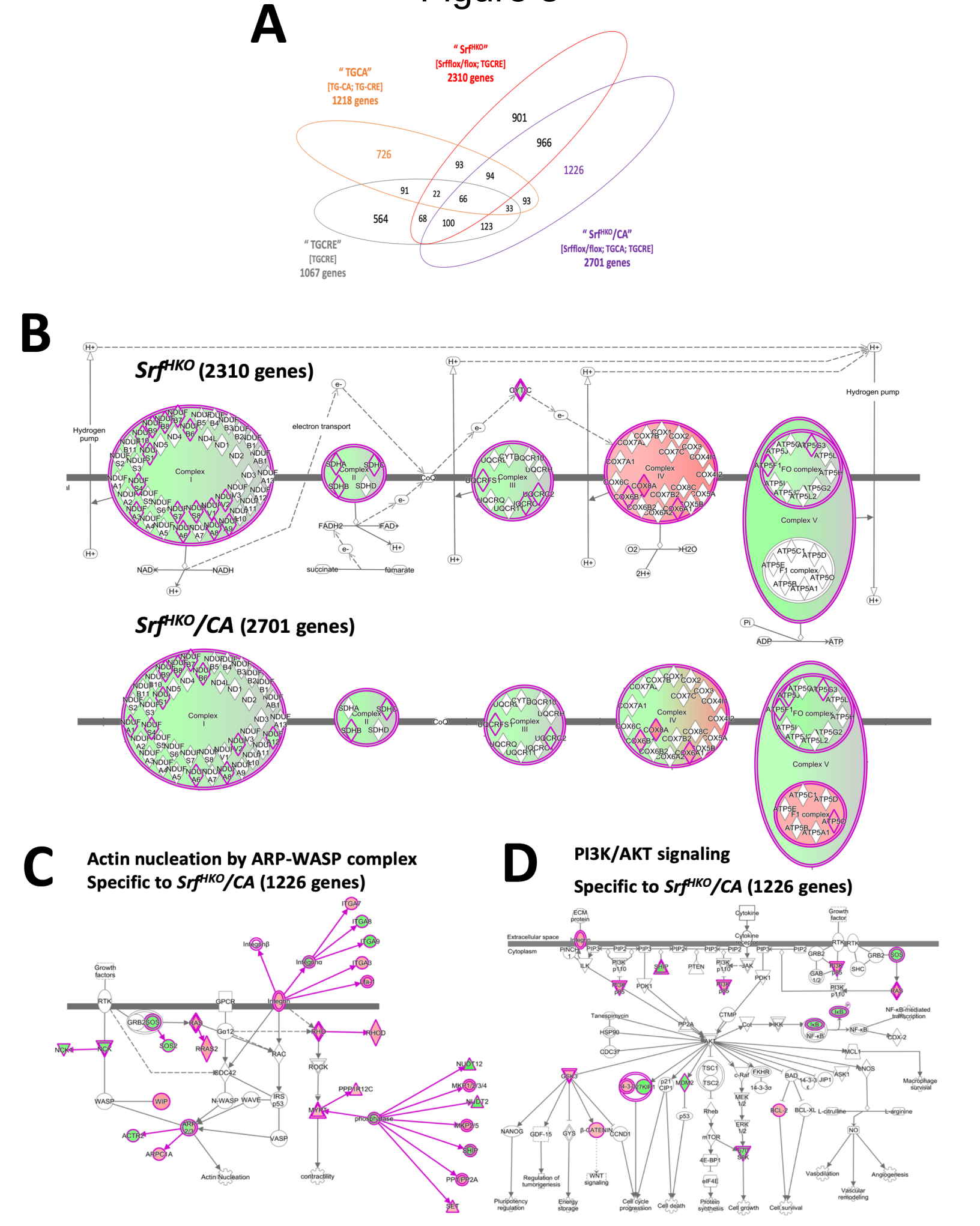
A
" TGCA"
[TG-CA; TG-CRE]
1218 genes
" SrfHKO"
[Srfflox/flox; TGCRE]
2310 genes
" TGCRE"
[TGCRE]
1067 genes
" SrfHKO/CA"
[Srfflox/flox; TGCA; TGCRE]
2701 genes
726
901
966
1226
93
94
91
22
66
33
93
564
68
100
123
B
SrfHKO (2310 genes)
SrfHKO/CA (2701 genes)
Hydrogen pump
electron transport
Complex I
Complex II
Complex III
Complex IV
Complex V
F1 complex
CoQ
CYTC
NAD
NADH
FADH2
FAD+
succinate
fumarate
O2
H2O
ADP
ATP
Pi
C
Actin nucleation by ARP-WASP complex
Specific to SrfHKO/CA (1226 genes)
Growth factors
RTK
GPCR
Integrin
Integrinβ
Integrinα
ITGA7
ITGA8
ITGA9
ITGA8
ITGA1
GRB2
SOS
SOS2
RAS
RRAS2
Gα12
RHO
RHOD
RAC
CDC42
ROCK
NCK1
PAK
WASP
WIP
N-WASP
WAVE
IRS p53
ARP 2/3
ACTR2
ARPC1A
VASP
Actin Nucleation
MYPT1
PPP1R12C
phosphatase
NUDT12
MKP1/2/3/4
NUDT2
MKP2/5
SHIP
PPP1/PP2A
SET
contractility
D
PI3K/AKT signaling
Specific to SrfHKO/CA (1226 genes)
ECM protein
Integrin
Extracellular space
Cytoplasm
Cytokine
Cytokine receptor
Growth factor
RTK
PINCH 1
ILK
PI3K p110
PI3K p85
SHIP
PTEN
JAK
PDK1
GRB2
SOS
SHC
GAB 1/2
RAS
Tanespimycin
HSP90
CDC37
PP2A
AKT1
CTMP
Cot
IKK
IκB
NF-κB
NF-κB-mediated transcription
COX-2
MCL1
eNOS
Macrophage survival
GSK3
14-3-3ζ
p21 CIP1
MDM2
TSC1
TSC2
c-Raf
FKHR
14-3-3σ
BAD
JIP1
ASK1
MEK 1/2
ERK 1/2
Rheb
mTOR
4E-BP1
eIF4E
p70 S6K
p53
BCL-2
BCL-XL
L-citrulline
L-arginine
NO
Vasodilation
Angiogenesis
Vascular remodeling
NANOG
GDF-15
GYS
β-CATENIN
CCND1
WNT signaling
Regulation of tumorigenesis
Pluripotency regulation
Energy storage
Cell cycle progression
Cell death
Protein synthesis
Cell growth
Cell survival

Figure 6

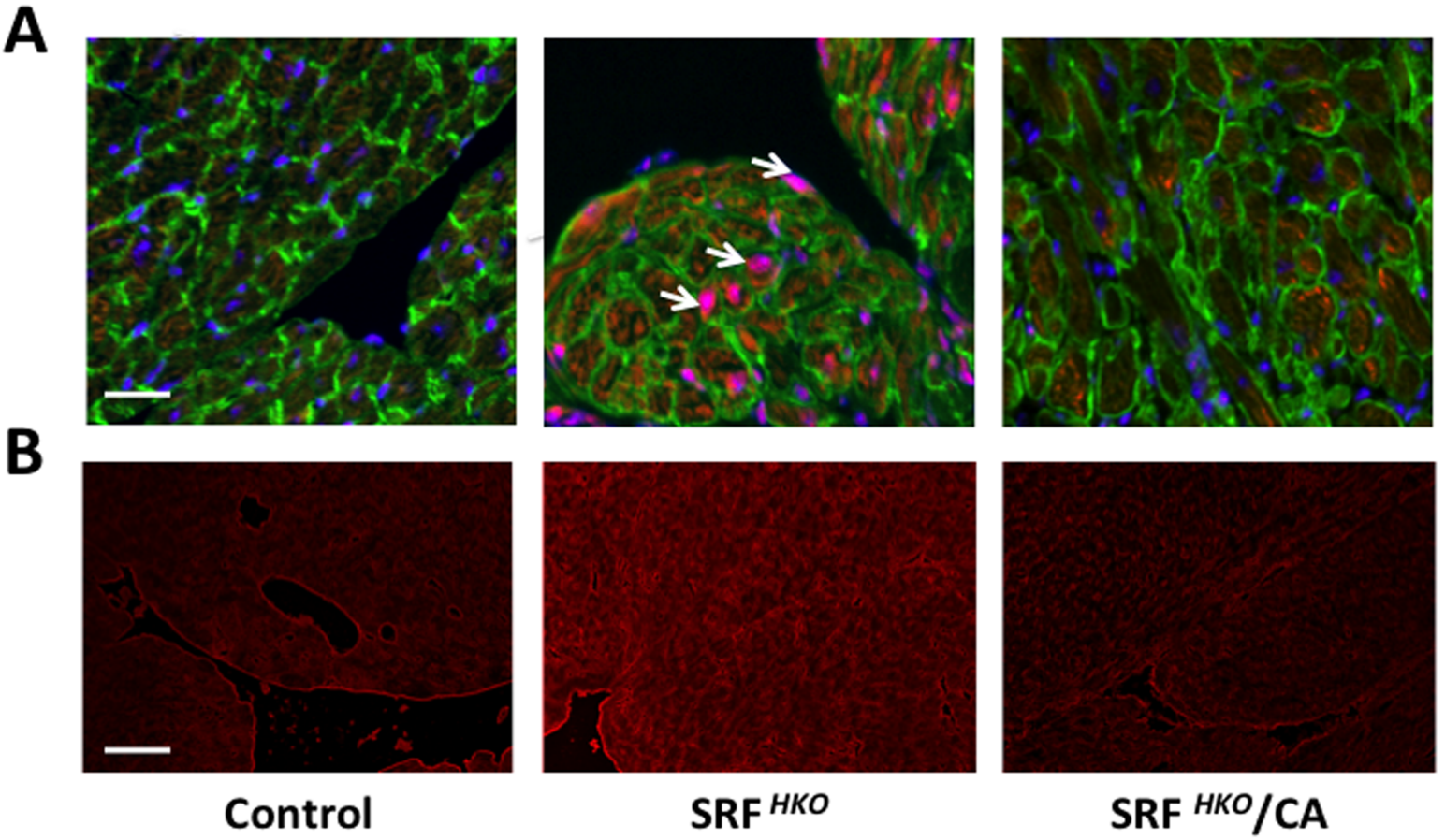
A
B
Control
SRF HKO
SRF HKO/CA

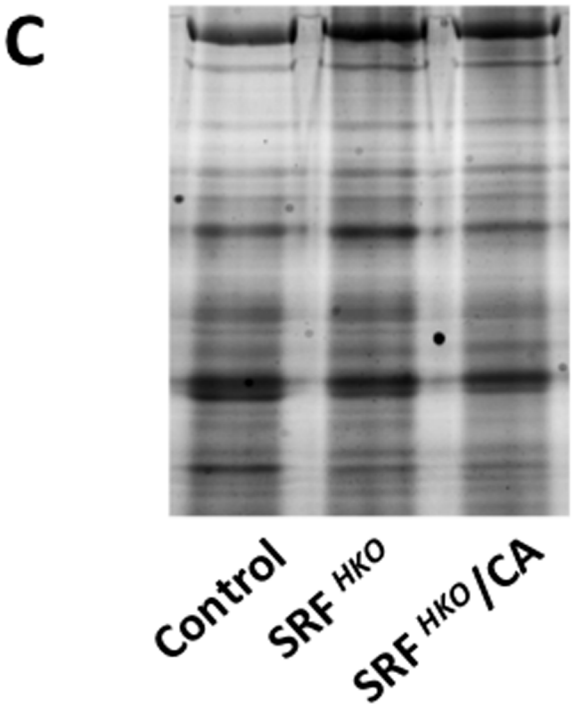
C
Control
SRF HKO
SRF HKO/CA

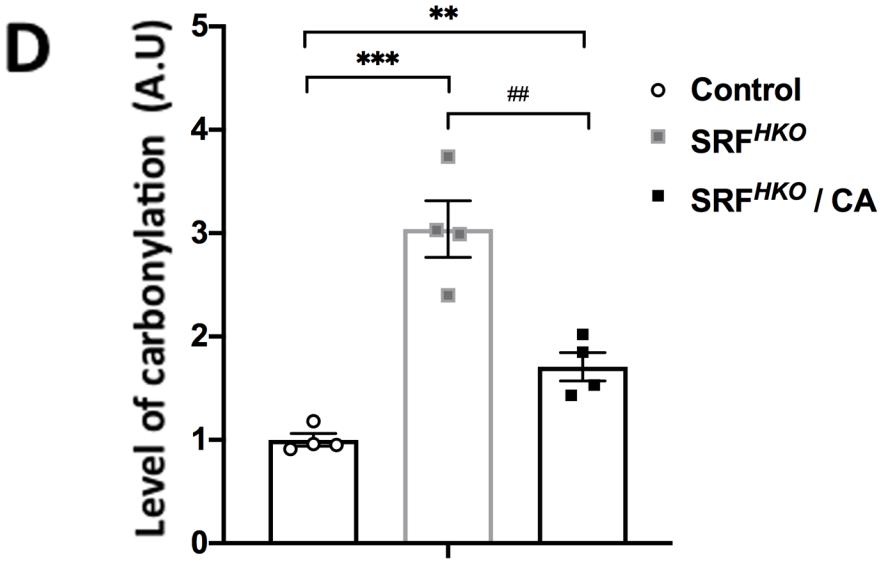
D
Level of carbonylation (A.U)
0
1
2
3
4
5
**
***
##
Control
SRFHKO
SRFHKO / CA

Figure 7

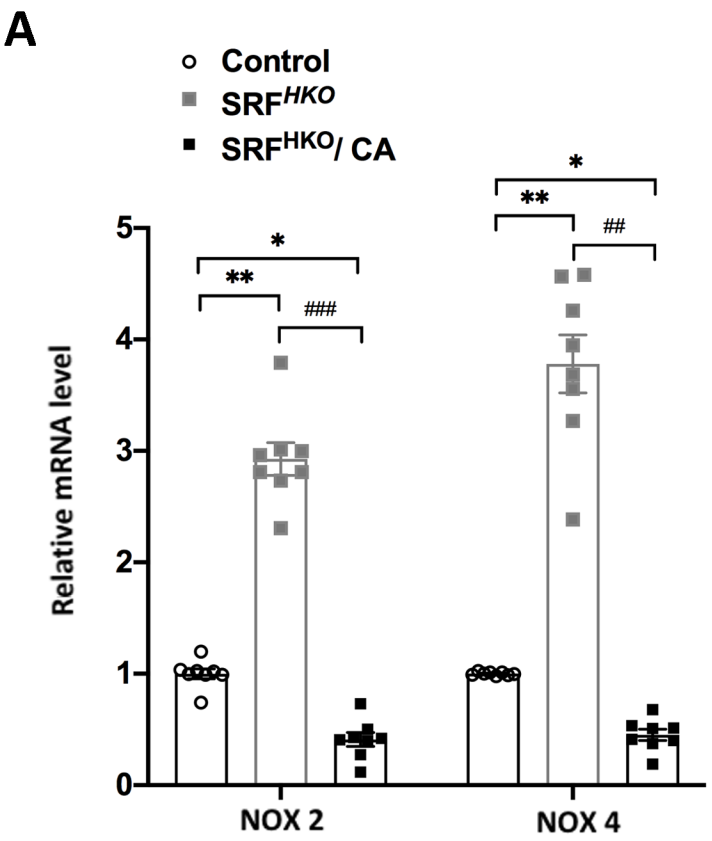
A
Control
SRF HKO
SRF HKO/ CA
Relative mRNA level
NOX 2
NOX 4
*
**
###
##

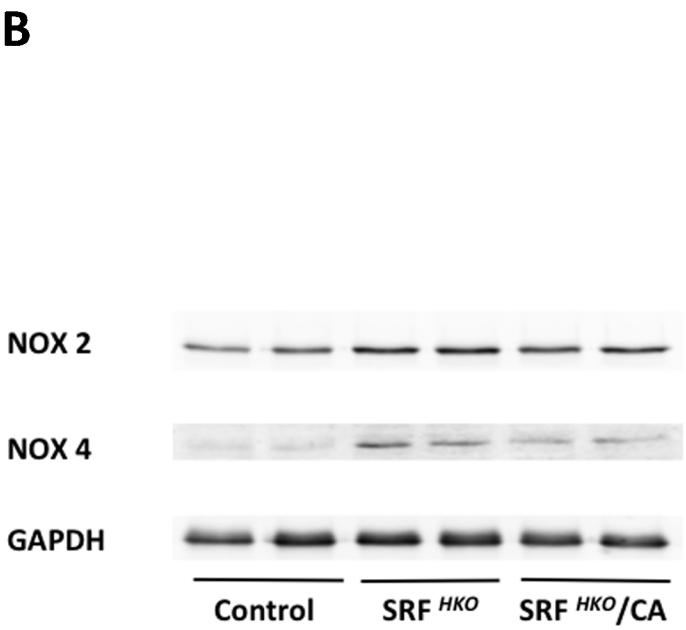
B
NOX 2
NOX 4
GAPDH
Control
SRF HKO
SRF HKO/CA

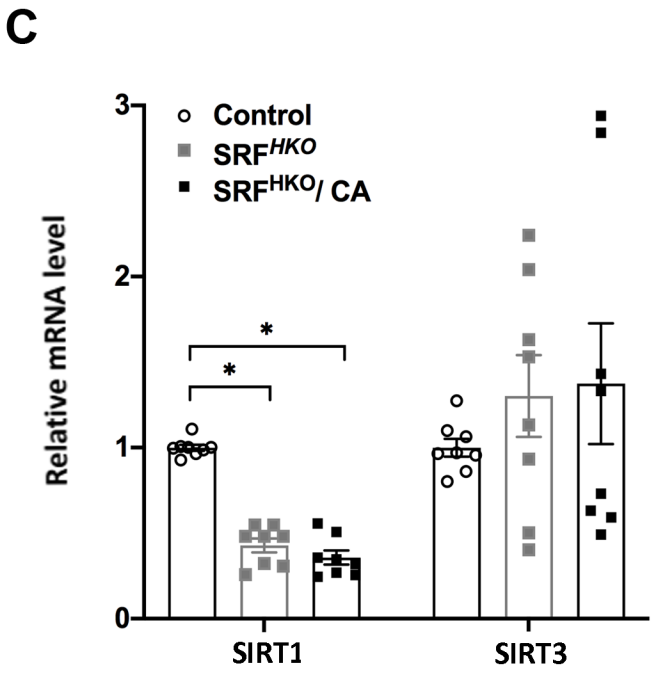
C
Control
SRF HKO
SRF HKO/ CA
Relative mRNA level
SIRT1
SIRT3
*

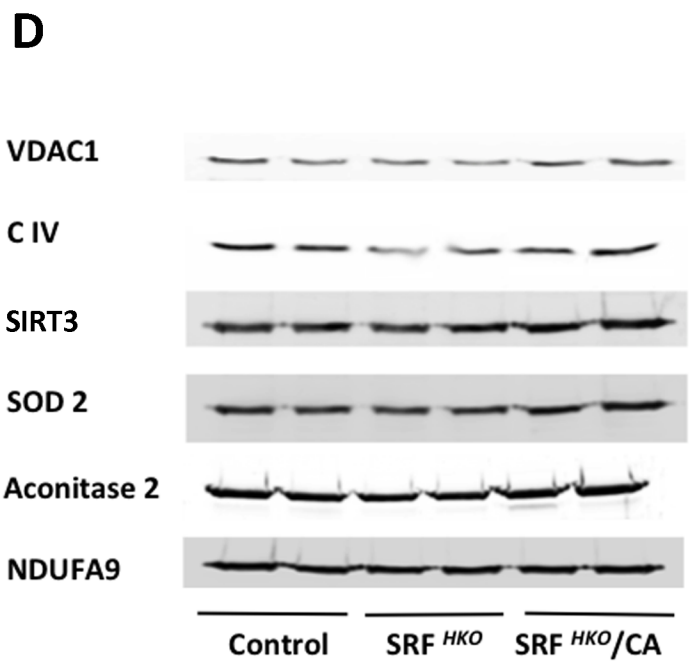
D
VDAC1
C IV
SIRT3
SOD 2
Aconitase 2
NDUFA9
Control
SRF HKO
SRF HKO/CA

Figure 8

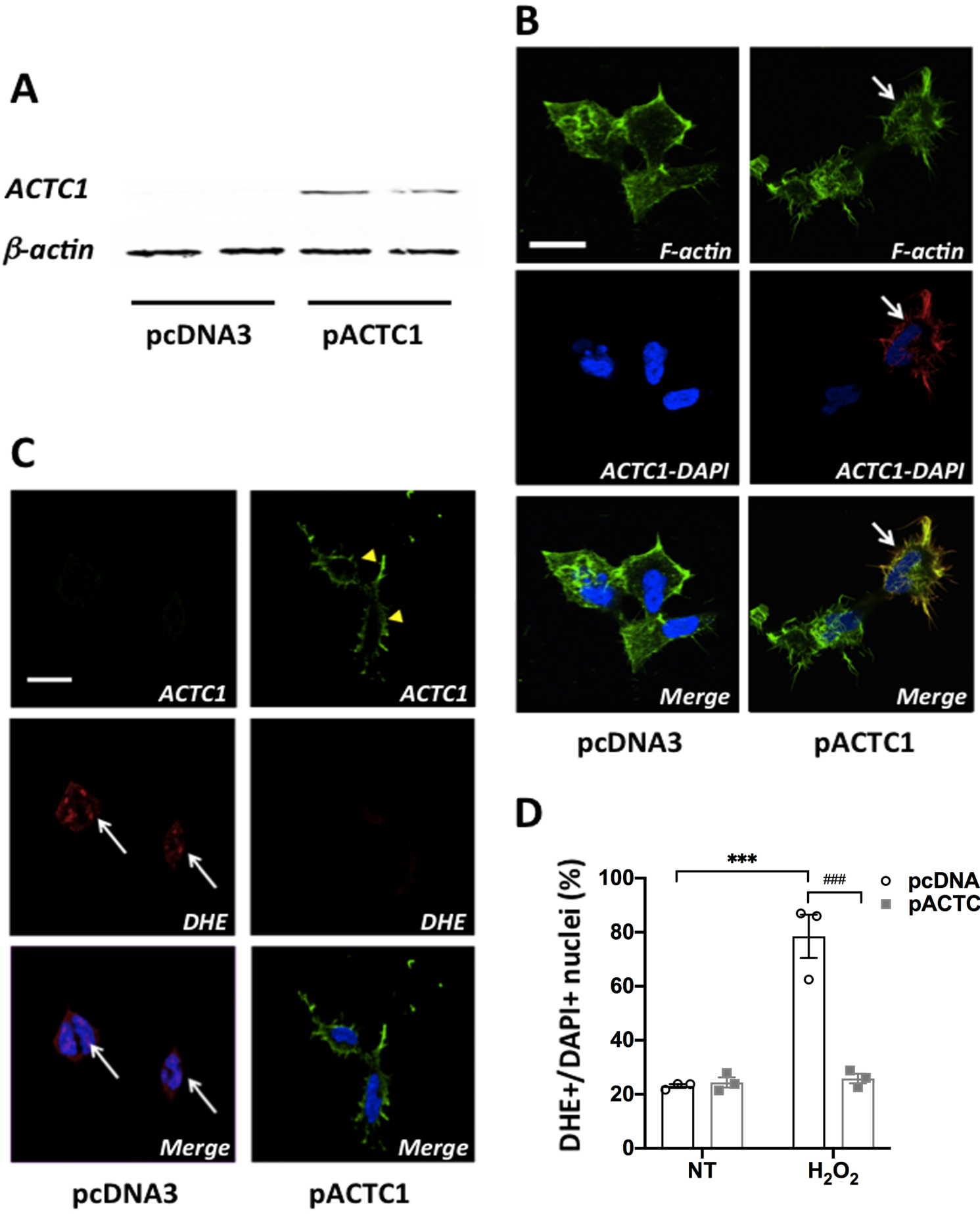
A
ACTC1
β-actin
pcDNA3
pACTC1
B
F-actin
F-actin
ACTC1-DAPI
ACTC1-DAPI
Merge
Merge
pcDNA3
pACTC1
C
ACTC1
ACTC1
DHE
DHE
Merge
Merge
pcDNA3
pACTC1
D
DHE+/DAPI+ nuclei (%)
100
80
60
40
20
0
***
###
pcDNA3
pACTC1
NT
H2O2

	Days after tamoxifen treatment					
	0			30		
	Control	**SRF HKO**	**SRF HKO / CA**	**Control**	**SRF HKO**	**SRF HKO / CA**
BW (g)	20.40 ± 1.56	20.10 ± 1.70	20.60 ± 1.41	20.80 ± 1.33	19.74 ± 1.04	21.51 ± 1.26
HR (bpm)	571.33 ± 15.76	556.80 ± 6.72	577.50 ± 16.70	597.00 ± 21.36	536.14 ± 18.94[a]	570.01 ± 14.33
h/r ratio	0.35 ± 0.01	0.34 ± 0.01	0.36 ± 0.03	0.31 ± 0.02	0.23 ± 0.01[a]	0.30 ± 0.02[b]
LVFWs (mm)	0.98 ± 0.04	1.04 ± 0.05	0.97 ± 0.03	0.95 ± 0.03	0.75 ± 0.02[a]	0.85 ± 0.03[a b]
LVFWd (mm)	0.52 ± 0.04	0.58 ± 0.05	0.50 ± 0.06	0.45 ± 0.03	0.51 ± 0.04	0.52 ± 0.03
EF (%)	81.65 ± 0.41	82.54 ± 0.49	82.03 ± 0.46	79.90 ± 0.18	44.14 ± 2.38[a]	65.24 ± 3.71[a b]
Vcfc (circ/s)	3.13 ± 0.09	3.02 ± 0.09	3,09 ± 0.07	3.00 ± 0.07	1.45 ± 0.13[a]	2.62 ± 0.17[a b]
Sa (cm/s)	2.83 ± 0.10	2.77 ± 0.13	2,86 ± 0.10	2.79 ± 0.09	1.99 ± 0.13	2.76 ± 0.14
Spw (cm/s)	2.95 ± 0.11	2.88 ± 0.09	2,92 ± 0.12	2.98 ± 0.08	1.75 ± 0.11[a]	2.51 ± 0.20[b]
E/Ea	16.8 ± 0.5	16.5 ± 0.5	16,7 ± 0.6	16.5 ± 0.5	22.8 ± 0.8[a]	16.4 ± 0.6[b]

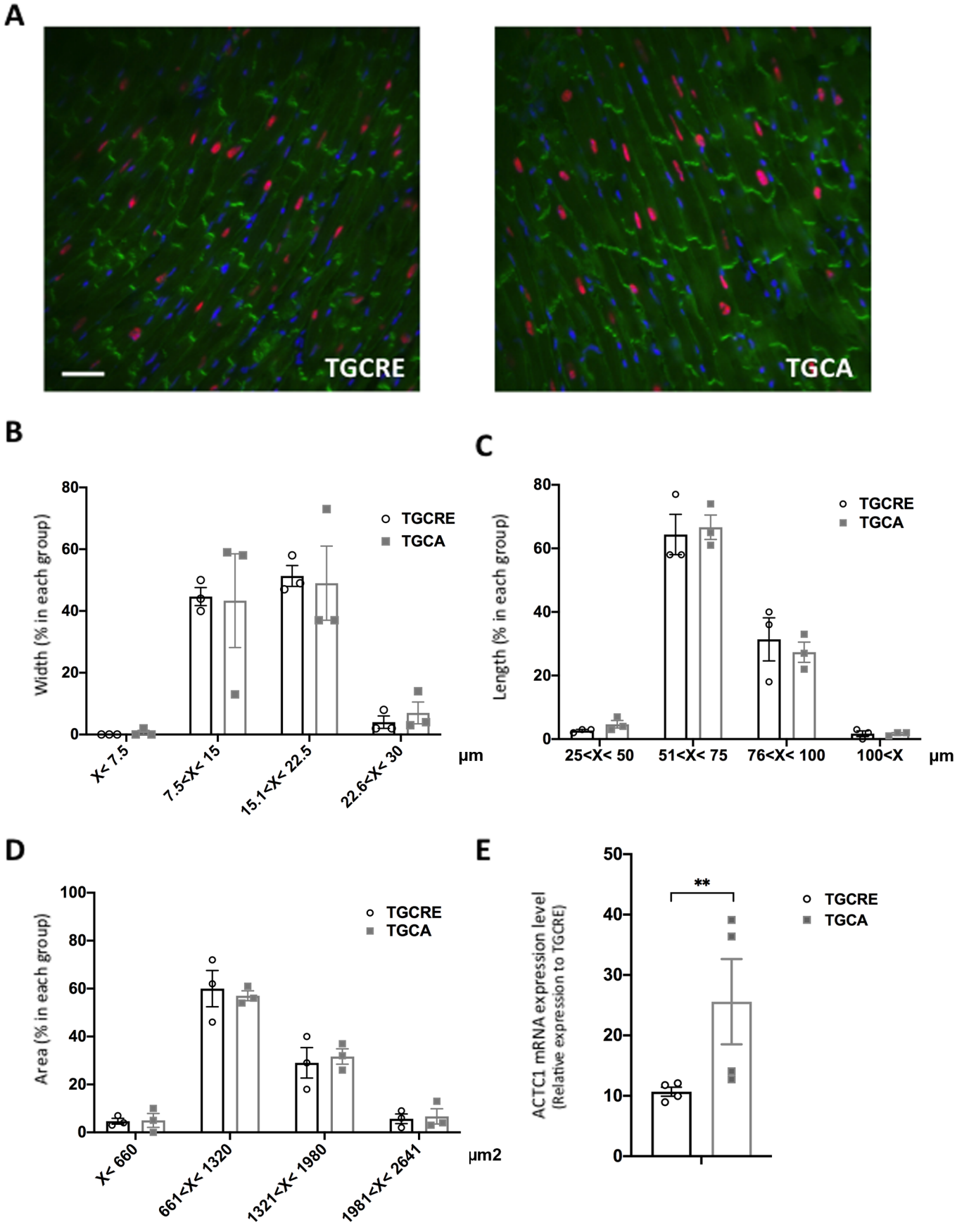

(A) Confocal microscopy of cardiac sections labelled with anti-vinculin FITC (green), anti-SRF (red) and DAPI (blue), scale: 30 µm. (B, C, D) Distribution of cardiomyocytes lengths, widths and areas in TGCRE and TGCA mice (200 cells/mouse, n=3). No significant difference was observed in the two groups whatever the parameters. (E) RT-qPCR analysis of ACTC1 mRNA (n=4), 30 days after tamoxifen treatment. Data are means ± s.e.m. ** indicates significant difference at $P < 0.01$ versus TGCRE. ACTC = α-cardiac actin; TGCRE = cre+card- +/+; TGCA = cre+ card+ +/+.

Top Canonical Pathways

Specific to *Srf^{HKO}* (901 genes)

Name	p-value	Overlap
Oxidative Phosphorylation	2,51E-03	9,2 % 10/109
Purine Nucleotides Degradation II (Aerobic)	2,69E-03	21,1 % 4/19
Neuregulin Signaling	2,83E-03	9,7 % 9/93
Urate Biosynthesis/Inosine 5'-phosphate Degradation	7,23E-03	23,1 % 3/13
Leukocyte Extravasation Signaling	8,50E-03	6,6 % 14/213

Specific to *[Srf^{HKO}/CA]* (1226 genes)

Name	p-value	Overlap
Phosphatidylcholine Biosynthesis I	1,26E-04	57,1 % 4/7
Choline Biosynthesis III	1,70E-04	38,5 % 5/13
PTEN Signaling	1,23E-03	11,4 % 14/123
Actin Nucleation by ARP-WASP Complex	1,68E-03	14,5 % 9/62
PI3K/AKT Signaling	1,95E-03	10,9 % 14/129

Common to *Srf^{HKO}* and *[Srf^{HKO}/CA]* (966 genes)

Name	p-value	Overlap
Mitochondrial Dysfunction	1,61E-09	15,2 % 26/171
Valine Degradation I	5,59E-09	50,0 % 9/18
Epithelial Adherens Junction Signaling	1,04E-08	15,4 % 23/149
Fatty Acid -oxidation I	1,37E-08	34,4 % 11/32
Sirtuin Signaling Pathway	8,19E-08	11,0 % 32/292

Specific to *TGCA* (726 genes)

Name	p-value	Overlap
BMP signaling pathway	2,70E-03	8,5 % 7/82
IL-10 Signaling	4,89E-03	8,7 % 6/69
Actin Cytoskeleton Signaling	7,08E-03	5,2 % 12/231
Clathrin-mediated Endocytosis Signaling	8,84E-03	5,3 % 11/209
Tight Junction Signaling	1,53E-02	5,4 % 9/168

Top canonical pathways enrichment

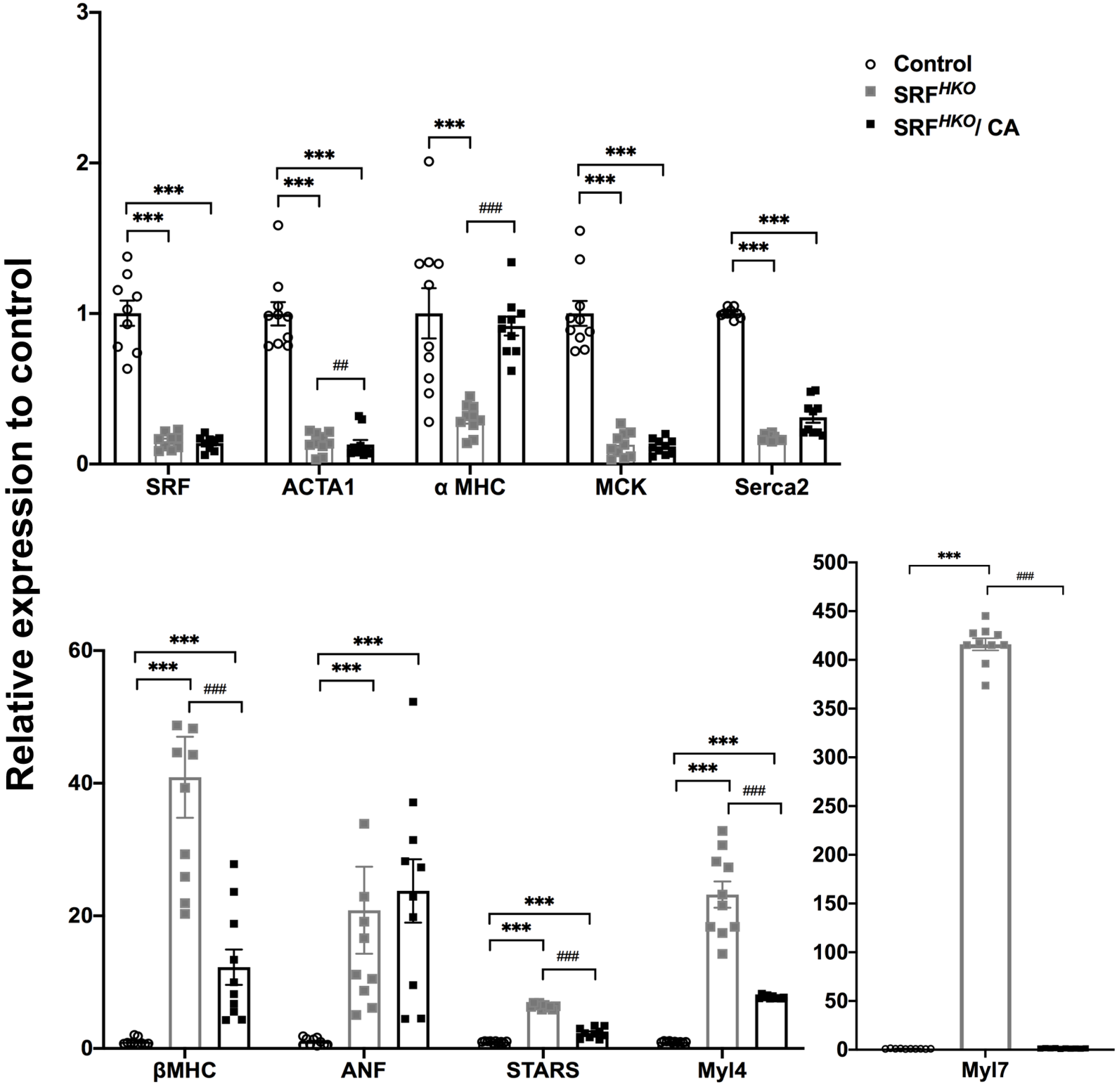

Impact of α-cardiac actin compensatory expression on gene expression.

Quantification of mRNA by RT-qPCR for the most representative SRF target genes and actin-associated protein coding genes in control (n=10), in SRF ^{HKO} (n=10) and SRF ^{HKO}/ CA (n=10), using cyclophilin A, SDHA and GAPDH as internal controls.

Data are means ± s.e.m. *** indicates significant difference at $P < 0.001$ versus the control group and, ## and ### at $P < 0.01$ and $P < 0.001$ versus the SRF ^{HKO} group.

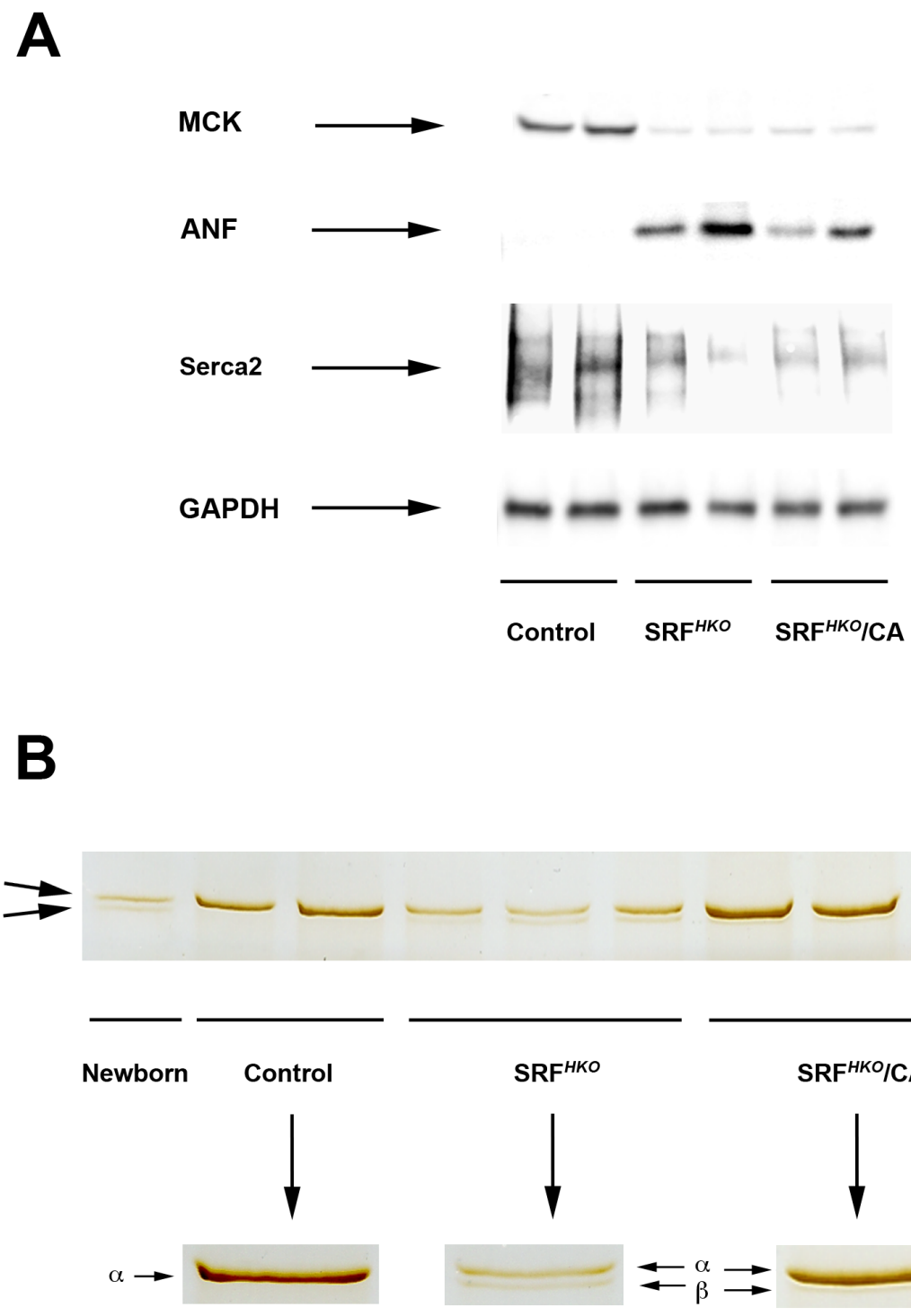

(A) Western blot analysis of MCK (43 kDa), ANF (28 kDa) and Serca2 (115 kDa) proteins in control, SRF ^{HKO} and SRF ^{HKO}/CA mice. These data are representative of two independent experiments. (B) Electrophoretic separation of cardiac muscle MHC in newborn, control (n=2), SRF ^{HKO} (n=3) and SRF ^{HKO}/CA (n=3) mice. 3 µg of proteins were used except in newborn (1 µg). In the newborn mouse heart both αMHC (upper) and βMHC (lower) were expressed whereas in the adult control αMHC was the only form to be detected. In SRF ^{HKO} hearts, βMHC is also expressed and a decrease of total MHC proteins is observed compared with the two other groups. However, in SRF ^{HKO}/CA hearts, βMHC is weakly detectable compared to αMHC protein expression.